Bioengineering.

Bioengineering
Individual Investigative Project

Design of a Microfluidic Device for the Magnetic Extraction of DNA

Saylee Jangam

May 2018

Dr Cécile M Perrault

Dissertation submitted to the University of Sheffield in partial fulfilment of the requirements for the degree of Bachelor of Engineering

Abstract

DNA extraction is an important first step in the detection of pathogenic DNA for the diagnosis of infectious diseases such HIV, Ebola, Chikungunya and Dengue Virus. While traditional DNA extraction methods require several centrifugation steps and are time-consuming, extraction carried out using magnetic nanoparticles offers a faster and more specific approach without the need for extensive laboratory equipment. The aim of this study was to test the feasibility of scaling down a magnetic nanoparticle-based DNA extraction method from the bench-top onto a lab-on-a-chip using MagSi-DNA beads (MagnaMedics Diagnostics BV). A novel six-chambered microfluidic device was designed that utilised 40X less reagent than on the bench-top, achieving extraction efficiencies of 9.7% for spiked solutions and 0.54% for the MG-63 cell model. DNA in an MG-63 cell was quantified using an approximation method (6.513 pg) and PicoGreen assay (7.350 pg) to calculate extraction efficiency (percentage throughput) from spectrophotometry results. Additionally, a limit of detection of 100 ng/µL was achieved using the MagSi-DNA beads on the bench-top.

Contents

Nomenclature

POC	Point-of-care
LOC	Lab-on-a-chip
DNA	Deoxyribonucleic Acid
RNA	Ribonucleic Acid
dsDNA	Double stranded DNA
PDMS	Polydimethylsiloxane
DENV	Dengue Virus
MNP	Magnetic Nanoparticle
PBS	Phosphate Buffer Solution
FCS	Fetal Calf Serum
MG-63	Osteosarcoma cell line
PCR	Polymerase Chain Reaction
BSA	Bovine Serum Albumin
PEG	Polyethylene glycol
SD	Standard Deviation (σ)
SE	Standard Error
A_{260}	Absorbance at 260 nm
A_{230}	Absorbance at 230 nm
A_{280}	Absorbance at 280 nm
$A_{260/280}$	Ratio of absorbance at 260 and 280 nm

$A_{260/230}$ Ratio of absorbance at 260 and 230 nm

1. INTRODUCTION

1.1 DNA Extraction in Diagnostic Platforms

The detection of pathogenic DNA (Deoxyribonucleic Acid) offers a specific and accurate way to diagnose infectious diseases such as HIV (Human Immunodeficiency Virus), Ebola, Chikungunya and Dengue Virus [1]. The first step in DNA detection is its extraction from bacterial or viral infection in human blood. As a result, DNA extraction forms an integral part of many diagnostic platforms that aim to directly detect pathogenic DNA, offering a highly specific and accurate diagnosis for a wide range of diseases.

As a first point of application, this study will focus on the Dengue Virus (DENV) which is endemic in subtropical regions of the world like Vietnam. DENV is spread through a vector – the *Aedes aegypti* mosquito – which thrives in heavy rain and high temperature conditions. The main challenge with DENV is that 80% of all patients are asymptomatic or show common flu-like symptoms and are therefore, under the risk of an incorrect diagnosis [2]. Patients are often mistreated with antibiotics, increasing the risk of disease progression and antibiotic resistance [3]. It is crucial to be able to detect DENV in its early stage of infection where it can still be prevented from developing into its more severe form, the Dengue Haemorrhagic Fever (DHF). Detection methods in clinical use for DENV require laboratory intervention which is time consuming and expensive [4]. There is therefore a need for a rapid, low-cost and accurate way of diagnosing DENV at its early stage and at the point-of-care.

Microfluidics is a technology that is utilised in point-of-care diagnostic solutions for the controlled delivery and manipulation of fluids at the micro-scale (µ-scale). It allows standard bench-top methods to be scaled down and replicated on lab-on-a-chip (LOC) devices, significantly reducing assay times, reagent volumes, and overall costs. This makes microfluidic technology an attractive platform to use in developing countries where laboratory resources are scarce. Subsequently, magnetic nanoparticles (MNPs) have recently gained popularity through commercially available DNA extraction kits [5] [6] [7]. Microfluidic devices focusing on the extraction of DNA using MNPs have previously been studied [8], however, no clinically accepted diagnostic tool for this exists yet. While Hansen et. al have used MagSi-DNA MNPs (MagnaMedics Diagnostics BV, The Netherlands) for DNA extraction from bacterial cells in whole blood, these particles

have not been tested on a microfluidic platform for on-chip extraction of DNA as a point-of-care solution.

1.2 Aims & Objectives

This study aims to create a prototype of a microfluidic device for the extraction of DNA using MagSi-DNA mf magnetic nanoparticles. The purpose of this prototype will be to establish a working DNA extraction method on-a-chip for further development into a point-of-care diagnostic platform for the Dengue Virus.

The objectives of this study are to:

- Optimize a bench-top DNA extraction method using magnetic nanoparticles
- Design and fabricate novel microfluidic chips for DNA extraction
- Test the feasibility of scaling down the bench-top DNA extraction method onto a microfluidic chip
- Assess the limit of detection

2. LITERATURE REVIEW

2.1 Extraction Methods

DNA extraction is an important process for many downstream applications such as genome sequencing, polymerase chain reaction (PCR) and the detection of pathogens. Broadly, the process of DNA extraction consists of four main stages, which include cell membrane lysis, DNA isolation, purification and amplification. DNA was first isolated by Miescher in 1869, where acid was used to precipitate DNA from a solution of lysed leukocyte cells [9]. Since then, many alternative methods of DNA isolation have been developed to facilitate laboratory experiments.

The gold standard for DNA extraction is the phenol-chloroform method which separates DNA, RNA, lipids and proteins into three different phases depending on their polarity. Water is more polar than phenol and therefore attracts DNA – a negatively charged molecule – into its aqueous phase. Proteins sit within an interphase between the aqueous and non-aqueous phases. The non-aqueous phase consists of RNA and lipids which are non-polar like phenol. The supernatant of this triphasic emulsion (*Figure 2.2*) can then be removed and further purified through the addition of ethanol which precipitates DNA out of the solution [8]. While this method is reliable, it requires several mixing and centrifugation steps that are time-consuming and can only be carried out in a laboratory-setting, limiting its portability to remote locations in developing countries. Additionally, the use of phenol poses safety hazards to laboratory workers, limiting its use to trained and experienced personnel [11].

Recognizing the need for a safe and rapid method of DNA extraction, Johns Jr. et al proposed using sodium perchlorate and chloroform in place of phenol-chloroform, to extract DNA from peripheral blood. In this study, Triton-X, a type of detergent solution, was used to lyse cells, avoiding the use of traditional proteinase K lysis methods which require overnight incubation for effective lysis [10]. The amount of DNA obtained with this method was comparable to that obtained from the traditional proteinase K and phenol-chloroform method, however, several centrifugation steps were still required for extraction.

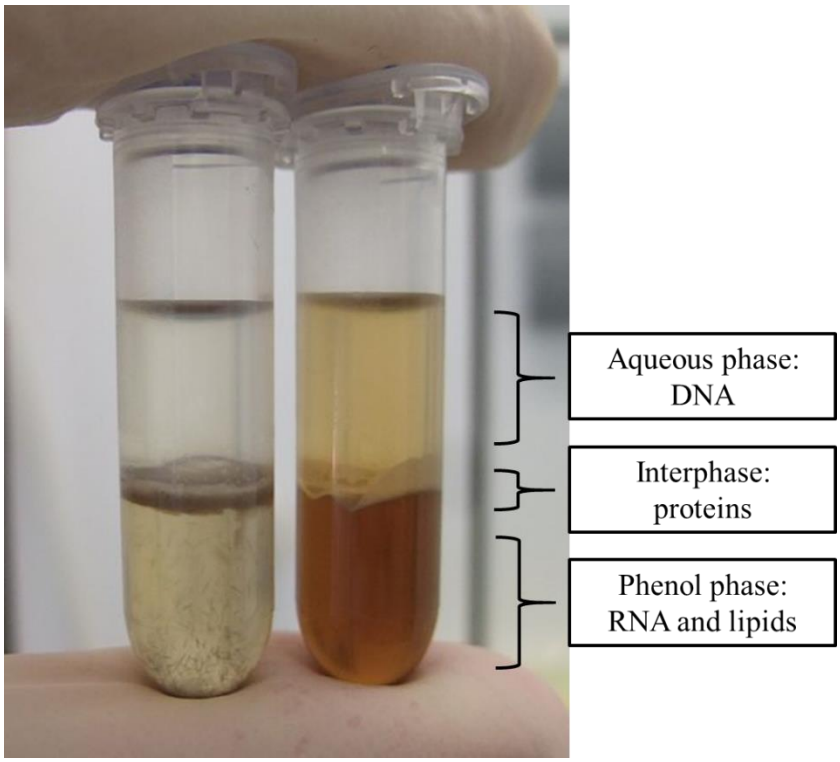

Figure 2.1.1 Tri-phasic emulsion in phenol-chloroform DNA extraction from mouse tail (L) and mouse liver (R) tissues [11].

More recently, solid-phase nucleic acid separation techniques have gained popularity due to their ease-of-use and availability on the market [12] [13] [14]. These techniques use silica matrices, glass beads, diatomaceous earth and magnetic nanoparticles as their "solid-phase". Solid-phase nucleic acid separation consists of cell lysis, DNA binding, washing to remove impurities, and the elution of DNA from the solid-phase matrix. The most common set-up for this type of extraction procedure is a spin column which is coated with silica or glass beads that have an affinity for the negatively charged DNA-backbone in the presence of chaotrophic salts and pH buffers. A chaotrophic salt is one which favours silica's selectivity for DNA by altering hydrogen bonding between the two. Yang et. al describe a spin column-based method coupled with silica particles that immobilize DNA on the particles' surface to purify DNA more effectively, through high capacity binding, minimizing the co-purification of any PCR (Polymerase Chain Reaction) inhibitors that is seen in the phenol-chloroform method [15]. PCR is a method which relies upon the purity of the DNA sample for effective replication, which is important for downstream applications.

Alternatively, Katevatis et. al argue that there are loss mechanisms associated with spin column-based methods which arise from DNA adsorption on column walls, thus limiting efficiency and DNA elution [16]. This is due to the adsorption and elution of nucleic acids not being well understood at low concentrations. To obtain a higher throughput of DNA in diagnostic systems, Katevatis et al. studied DNA-silica adsorption at different pH levels (pH 3.0, 5.2, 8.0) with and without the presence of the chaotrophic salt, guanidium thiocyanate (GuSCN), finding that DNA adsorbed best at low pH in GuSCN. This study replaced the spin column with silica particles that were separated from the liquid-phase using a centrifugal filter (*Figure 2.1.2*).

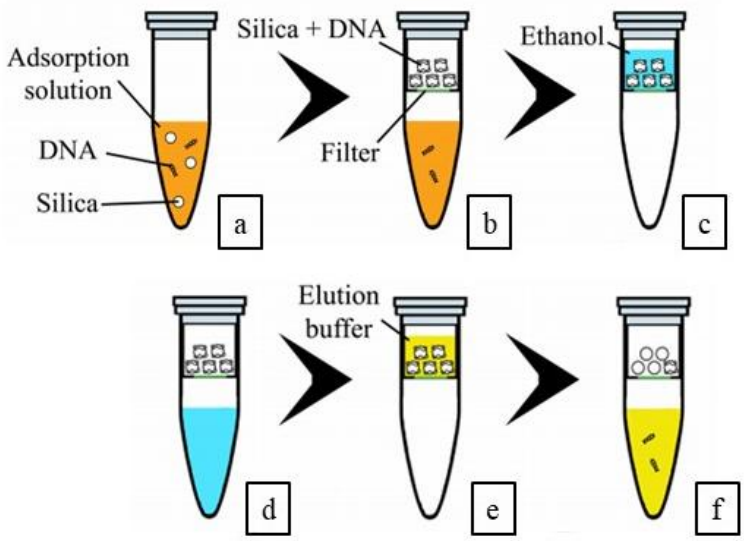

Fig 2.1.2 Schematic representing the sequence of steps in DNA extraction performed using silica beads and a centrifugal filter; a) Incubation, b) Lost DNA, c) Ethanol wash, d) Dry via centrifuge, e) Incubation, f) Recovered DNA (Katevatis et. al) [16].

Silica-coated magnetic nanoparticles (*figure 2.1.3*) negate the need for centrifugation and filtration steps as they can be separated from the solution by an external magnetic field [17]. This significantly reduces the time taken for the DNA extraction process, with opportunity to be applied to rapid diagnostic platforms.

As opposed to the liquid-phase separation, solid-phase separation techniques overcome the challenges associated with incomplete phase separation in liquid-phase extraction, providing a faster and more efficient way of extracting nucleic acids.

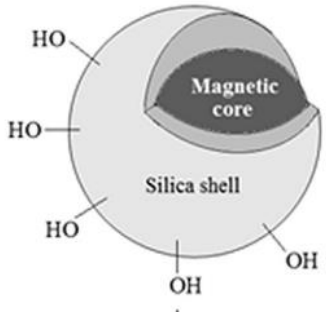

Fig 2.1.3 Iron (II) oxide core of magnetic nanoparticle coated with silica SiO2 (Wierucka et. al, 2014) [17].

Saiyed et. al developed a MNP-based DNA extraction method to isolate genomic DNA from whole blood with a mean particle size of 40 nm [18]. The protocol took 15 minutes to operate as opposed to the several hours taken by the phenol-chloroform method. Additionally, this method produced pure DNA, ready for amplification by PCR, and did not require the use of organic solvents or expensive equipment, making it more attractive in the POC diagnostics arena. Saiyed et. al highlight that magnetic methods refrain from applying mechanical stress to analytes which could be damaging, as is seen in other methods. With magnetic extraction of DNA being quick, inexpensive and robust, the opportunity for miniaturization into microfluidic volumes and the capability of scaling-up and automation is huge [18]. However, this method is limited to being conducted on the bench-top and requires at least 30 µL cell solution to produce PCR-ready DNA. For a microfluidic platform, this is a relatively high volume and needs to be scaled down even further which the prototype in this study aims to do.

In another study, Min et. al coated MNPs with dimercaptosuccinic acid (DMSA), effectively conjugating carboxyl groups onto the surface of the particles to adsorb DNA. DNA was isolated from whole blood using these and compared with a commercially available kit, where the DMSA-treated particles showed greater DNA recovery than the commercial beads through gel electrophoresis (*Figure 2.1.4*) [19].

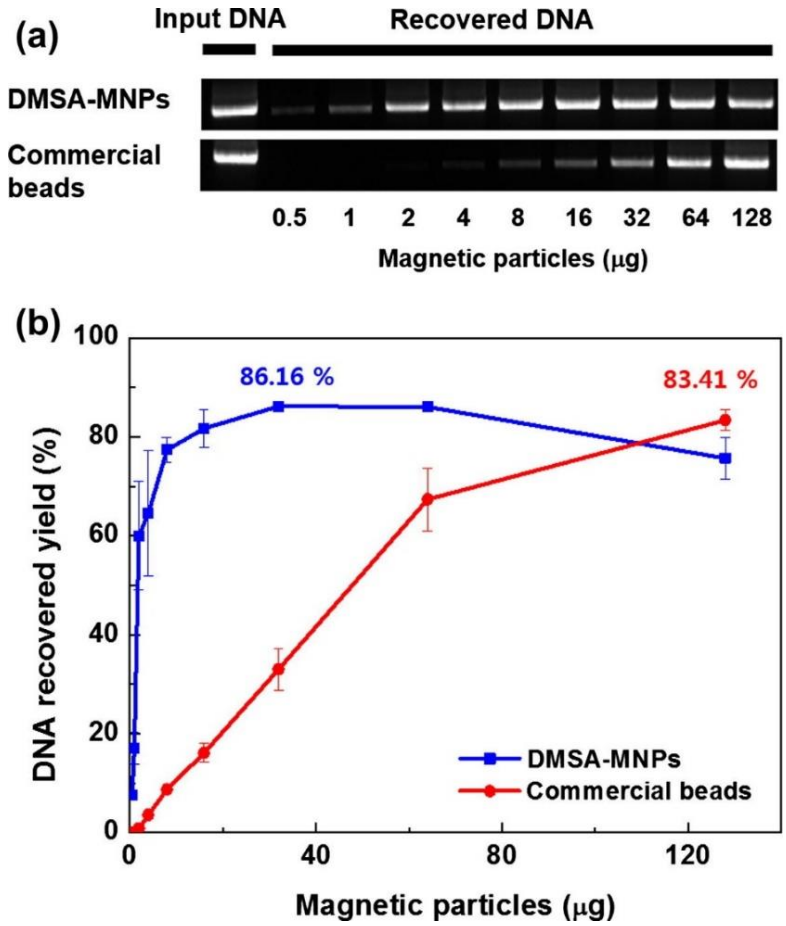

Figure 2.4.1. A comparison of DNA yield between DMSA-treated MNPs and commercially available kits. (a) Agarose gel electrophoresis showing greater DNA recovery by DMSA-MNPs than commercial beads and (b) DMSA-MNPs showing higher affinity for DNA at lower concentrations than commercial beads (Min et. al, 2014) [19].

Hansen et. al used the same magnetic nanoparticles as used in this study (MagSi-DNA, MagnaMedics Diagnostics BV) to extract DNA from whole blood on the bench-top, subsequently identifying the need to remove PCR inhibitors from DNA samples for more effective detection of bacterial pathogens [32]. By applying a "pre-analysis" treatment to the samples, a detection of 50 CFU (colony-forming unit) per mL of whole blood was obtained, which was comparable to the detection made using conventional phenol-chloroform methods.

2.2 Detection Methods

A variety of detection methods can be used in DNA extraction, right from UV spectrophotometry and gel electrophoresis, to mass spectrometry and fluorescent tagging of nucleic acids. In studies conducted by Saiyed et. al and Min et. al, agarose gel electrophoresis and UV spectrophotometry methods were used complimentarily to confirm the presence of DNA and the purity of the yield [18] [19]. Gel electrophoresis is visual technique that separates DNA fragments based on size and charge. An electric current is passed through the gel which separates the negatively charged DNA-fragments into separate bands across the length of the gel. DNA can be collected from the gel and further purified for more specific downstream analysis. Additionally, the lack of smears in the gel is used to confirm the absence of any RNA or protein contamination in the sample [19].

On the other hand, UV spectrophotometry provides a quantitative method to detect DNA, albeit non-specific. Using the Beer-Lambert Law, a spectrophotometer can relate a sample's optical density to its concentration. Nucleic acids absorb intensely at specific wavelengths, with DNA and RNA both absorbing highest at 260 nm. By manipulating the Beer-Lambert Law (Equation 2.1), the concentration of a DNA sample can be calculated if the absorbance value (A) at 260 nm (A_{260}), the pathlength of the spectrophotometer (b), and the extinction coefficient (E) are known. For dsDNA (double stranded DNA) at 260 nm, the extinction coefficient is 50 ng/µL at a pathlength of 1 cm [20].

2.2 $$c = \frac{A}{E \times b}$$

The Beer-Lambert equation [34].

In the Nanodrop (*Figure 2.2.1*), the pathlength is automatically adjusted to operate between 0.05 and 1.0 mm, which is significantly shorter than larger spectrophotometers that use cuvettes and pathlengths of 10 mm to calculate absorbance. Another method of quantifying DNA is by using a standard curve to relate absorbance with known concentrations of lambda (bacterial) or calf thymus DNA. While the Nanodrop

spectrophotometer minimizes sample volumes by over a 10-fold and can measure more concentrated samples due to its shorter pathlength, it brings with it challenges such as greater risk of light scattering within the sample and error to the non-specific absorption of light by molecules. Additionally, the ratio of absorbance values at 260 nm (A_{260}) and 280 nm (A_{280}) is used to identify the presence of DNA, and the ratio of absorbance values at 260 nm (A_{260}) and 230 nm (A_{230}) is used to assess the purity of the nucleic acids present. Standard curves can then be used to relate A_{260} values to specific DNA concentration using the Beer-Lambert law.

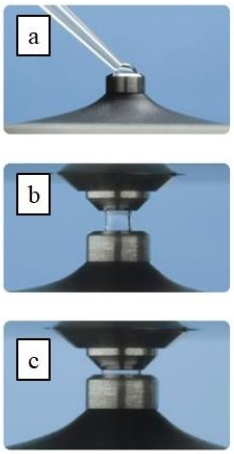

Fig 2.2.1a) 1-2 µ sample pipetted onto pedestal, b) Sample column, c) Pathlength adjusted to 0.05-1 mm. [21] (ThermoFisher Scientific, UK).

Fluorescent dyes help overcome some of the challenges seen with the non-specific absorption of molecules in 260 and 280 nm range and can be used to quantitatively assess the presence of DNA at very low concentrations. Commonly used dyes for DNA staining include SYBR Green I, Hoechst and PicoGreen, of which PicoGreen has the highest sensitivity, detecting between 50 pg and 2 µg DNA [22].

2.3 Microfluidic Design

Lab-on-a-chip (LOC) devices use microfluidics to scale-down reagent volumes, increase assay times and reduce costs. LOCs aim to mimic standard bench-top methods on microfabricated chips for precise and controlled liquid delivery. Many biosensors now use this technology to provide point-of-care diagnostic solutions in the clinic. This is particularly useful in the developing world where expensive laboratory settings are difficult to source.

Chand et. al report a microfluidic chip that electrochemically detects noroviruses using pulse voltammetric analysis which delivers a potential difference to the analytes and records the current generated. In this study, specific detection was obtained by functionalizing the gold nanoparticles with capsid-specific aptamers [23]. The time taken for detection of norovirus in spiked blood was less than 35 minutes and the limit of detection was 100 pM. Using CMOS (Complementary Metal-Cxide Semiconductor) technology, Toumazou et. al developed a label-free, non-optical and real-time method for detecting and quantifying target sequences of DNA by monitoring pH changes caused by the release of hydrogen ions during nucleotide base-pairing [24]. On the same chip, amplification of target sequences was achieved through incorporation of ISFET (Ion Sensitive Field Effect Transistor) arrays, embedded heaters and temperature sensors, thereby eliminating the need for external thermocycling equipment [24].

Cho et. al developed a lab-on-a-disc device that facilitates the targeted lysis of pathogens on a CD. Using streptavidin-conjugated MNPs with biotin-conjugated pathogen-specific antibodies (*Figure 2.3.1*), the pathogen was specifically lysed using laser irradiation. Irradiation causes the pathogens to lyse and release their DNA [25].

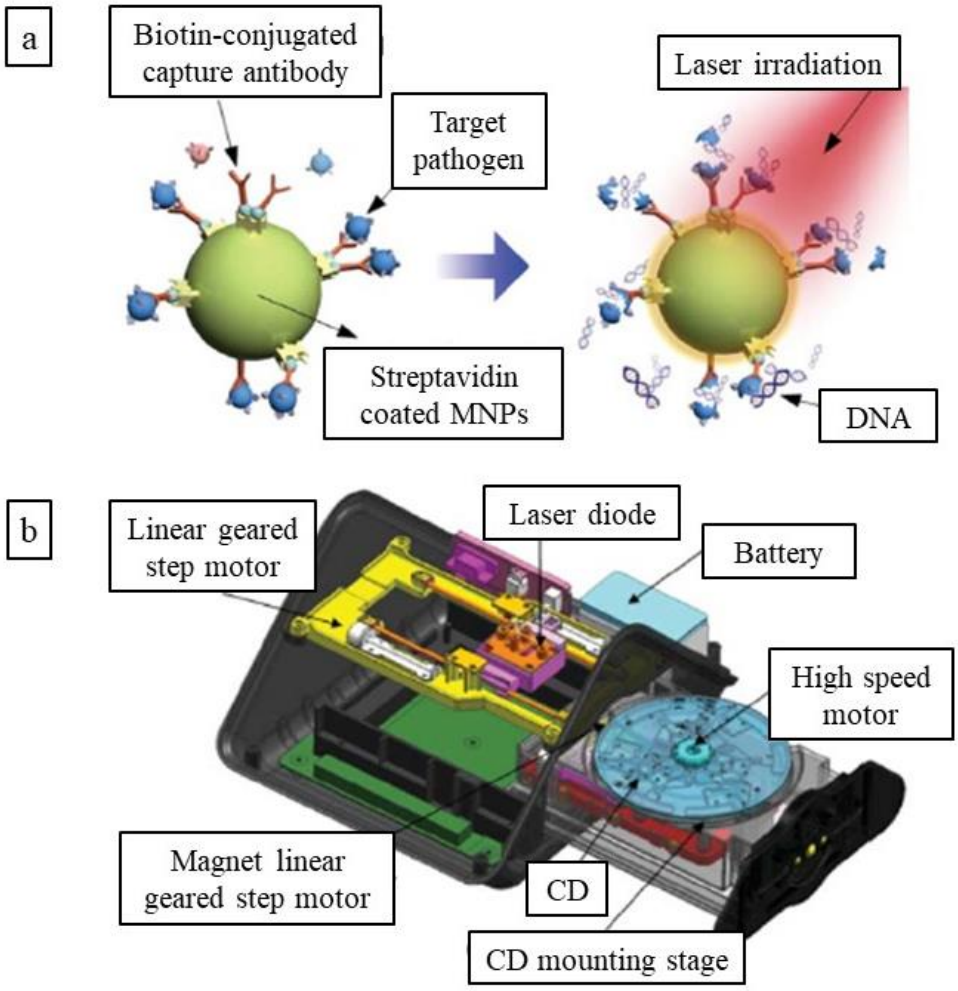

Fig 2.3.1 A lab-on-a-disc platform capable of (a) DNA extraction using antibody-conjugated MNPs and laser irradiation (808 nm, 1.5 W) and (b) the portable device with a laser-irradiated magnetic bead system (LIMBS) and a single laser diode operating ferro-wax microvalves by Cho et. al [25].

As opposed to this, Hong et. al developed a traditional PDMS microfluidic chip for the detection of mRNA and DNA using multilayer soft lithography. The use of this method allowed the fabrication of more robust micromechanical valves, preventing the risk of cross contamination and leakage between the different chambers of the device [26].

Iranmanesh et. al introduce a novel microvortexing method that can be conducted on a microfluidic chip [27]. This study has shown the importance of effective mixing in assay successfulness, which is easily overlooked on the smaller scale of a microfluidic chip where reaction times are much faster. While it is possible to mix using a pipette or a

vortexing machine on the lab bench, it is not feasible to do so with the chip because this can disturb flow, causing backflow or even leakage from chambers due to aggressive mechanical stimulation. Iranmanesh et. al have described microvortexing as being useful for resuspension of the magnetic bead pellet, which is required in the elution chamber of the design produced in this study. The method uses an external ultrasound horn transducer (*Figure 2.3.2*) that focuses onto the microfluidic chip, with a fixed-frequency electronic driver board that actuates the vortexing movement. The vortexing can be optimised for different functions, including cell lysis and DNA extraction. However, this method is limited to PMMA chips which are more rigid than PDMS equivalents, the latter of which are likely to tear through mechanical forces posed by microvortexing. To have the same flexibility as PDMS and be robust against mechanical forces, Flexdym could be used, which is an elastomer developed by Lachaux et. al to replace PDMS in microfluidic chips.

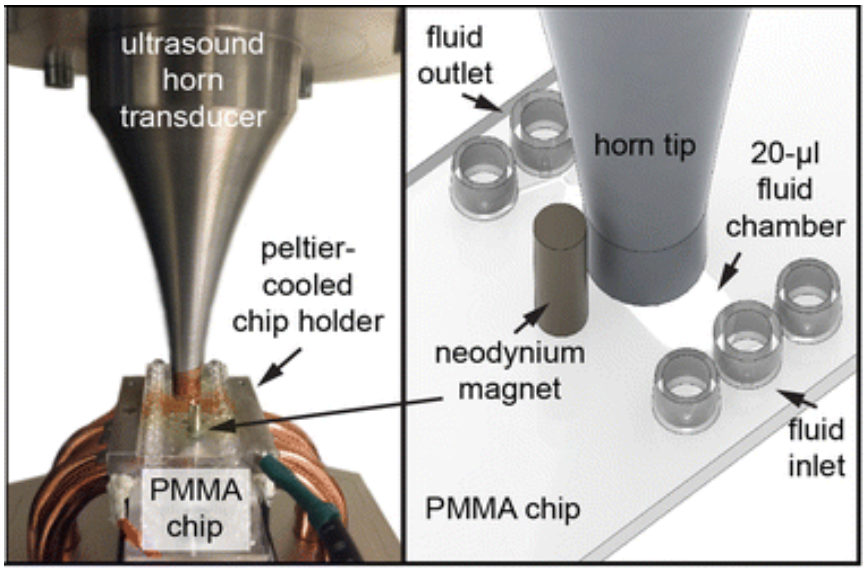

Figure 2.3.2 A microvortexing device for PMMA microfluidic chips (Imranmanesh et. al) [27].

The mixing in microfluidic systems is characterised as being either passive or active. Passive microfluidic systems do not utilize any external energy coming from a pump or other mechanical device, but instead use pressure differences within the device and capillary forces to drive flow. The advantage of using passive systems is that they require less equipment and are self-reliant [28]. However, they are limited in their applications due to the inability to precisely control flowrate. Additionally, active

microfluidic systems, such as the one developed by Schilling et. al, can remain relatively uncomplex depending on the equipment used [29]. Two pumps controlling inlet and outlet flows were used in this study to separate DNA and protein from cell lysate based on their size differences. However, the application of active systems in a diagnostic platform such as the prototype developed in this study, is more difficult to incorporate due to the multiple inlet/outlet chambers.

Capillary microfluidics are a type of passive microfluidic system that rely on capillary tension to drive flow within the system. Safavieh et. al introduced two novel microfluidic capillary elements – retention burst valves (RBVs) that stop liquid from flowing into the next chamber by build-up of large capillary pressure, and robust low aspect ratio trigger valves (TVs) which need a trigger from the second liquid for the first liquid to flow – the incorporation of which allows the creation of an autonomous and self-powered device, undergoing a defined sequence of steps after sample addition without the need of external pumps (*Figure 2.3.3*) [30].

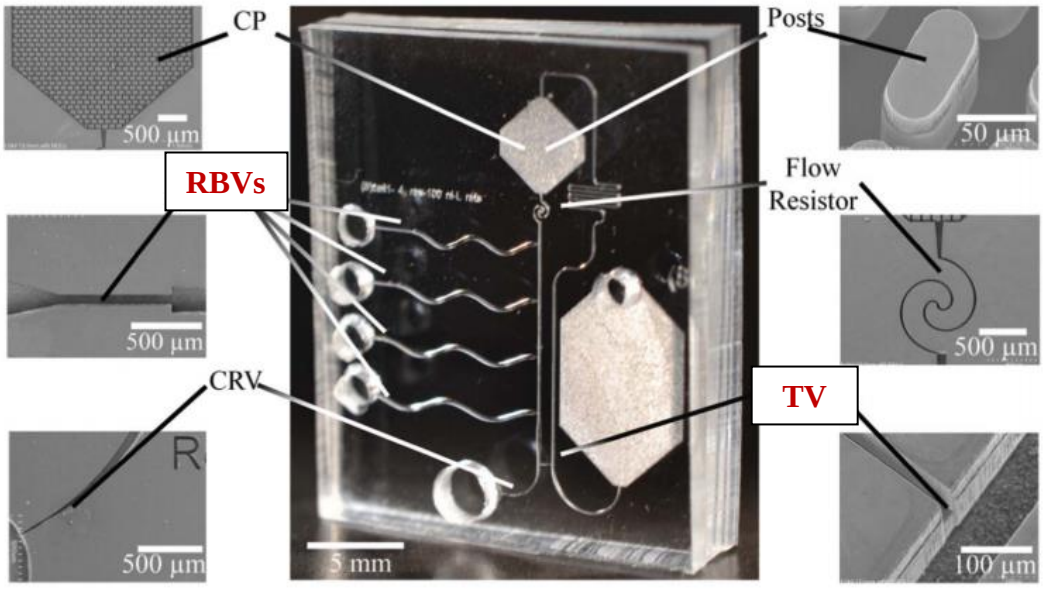

Figure 2.3.3 A self-powered microfluidic system based on capillary tension showing RBVs (Retention Burst Valves) and TVs (Trigger Valves) (Safavieh et. al, 2013) [30].

2.4 Current Dengue Virus Diagnostics

Dengue virus levels (viremia) levels in blood differ significantly from patient to patient, with primary infections resulting in higher viremia levels than secondary infections, and the type of dengue virus (DENV1-4) influencing this too. The general range observed in a study conducted in Mexico was 0.32–267,516 PFU eq/mL (Plaque-forming unit) for DENV-1 infections and 0.30–124,097 PFUeq/mL for DENV-2 infections [31]. The lower end of these ranges is difficult to detect using fluorescence or spectrophotometry and point to the need for an amplification system within the lab-on-a-chip device.

Point-of-care dengue diagnostics currently available on the market detect levels of NS1 (non-structural 1) antigen as well as IgG and IgM antibodies [32] [33] [34] [35]. Although being far from microfluidics, these rapid diagnostic tests (RDTs) have shown a large range of sensitivites (48.5 – 92.9%) and specificities (46.3 – 99.4%), however, they do not directly detect the presence of the viral pathogen, DENV [36]. *Figure 2.4.1* is an image of the Panbio Dengue Duo Cassette which measures the levels of both NS1 antigen and IgM antibodies. In comparison between all RDTs in the study by Blacksell et. Al , a clear advantage was seen in combining antigenic and antibody detection in the Panbio Cassette, demonstrating better accuracy [36].

Figure 2.4.1 Panbio Dengue Duo Cassette (Inverness, Australia) [20].

3. METHODS AND MATERIALS

3.1 Cell culture and suspension

All cells used in this study were taken from the MG-63 cell line at Passage-30 (see Appendix 1 for more information). Cells were cultured in Lonza Alpha-MEM (Minimum Essential Medium) with 10% FCS (Fetal Calf Serum) and Pen-Strep antibiotic. They were cultured in 75 mL flasks and incubated overnight at 37°C and 5% CO_2. Following overnight incubation, all media was removed from the flasks and the cells washed twice with 8 mL PBS (Phosphate Buffer Solution). 2.5 mL trypsin was then added to the cells to detach them from the flask, and the flask incubated for 5 minutes. Next, 5 mL media was added to the flask to stop trypsinization. The floating cells were counted on a haemocytometer to create the stock solution, which required concentrating the cells to 150 cells/µL for method 1, and 15,000 cells/µL for methods 2 and 3.

3.2 Bench-top DNA Extraction

All buffers and magnetic nanoparticles (MNPs) used in this protocol were part of the MagSi-DNA Pathogen Kit sourced from MagnaMedics Diagnostics BV (The Netherlands).

200 µL stock solution (cells) was transferred into three separate Eppendorf tubes to create Sample 1 (S1), Sample 2 (S2) and Sample 3 (S3). 150 µL lysis buffer was added to each tube and mixed using a pipette. MNPs were homogenised using an ultrasonic bath (Ultrasound Cleaning Bath, VWR Collection) for 5 minutes. 20 µL beads were added to each tube, followed by 440 µL binding buffer. The sample was then mixed using a pipette and incubated at room temperature for 10 minutes. The beads were then collected using a neodymium magnet (Amazon, UK) and the supernatants removed as efficiently as possible, using a pipette. 200 µL wash buffer-I was added and mixed. The beads were then collected using a neodymium magnet and the supernatant wash buffer removed as efficiently as possible, using a pipette. The washing step was repeated using 200 µL wash buffer-II and the supernatants removed. Following this, the tubes were dried with opened lids for 10-15 minutes. The volume of elution buffer used, and the temperature of elution depend on the version of the method followed during

optimisation (see Table 3.2.1). Either 40 or 100 µL elution buffer was added and the magnetic beads resuspended by pipetting up-and-down 5 times. Next, the samples were incubated at either room temperature or 42°C for 10 minutes. The beads were then collected using a neodymium magnet and the DNA supernatant transferred into new Eppendorf tubes as efficiently as possible, using a pipette. These samples (S1, S2 and S3) were then analysed using a Nanodrop-1000 Spectrophotometer (ThermoFisher Scientific, UK) following manufacturer's instructions.

This was then repeated with spiked solutions of calf thymus DNA at concentrations of 10 and 100 ng/µL, where method 3 was followed.

Method	**Number of cells per µL**	**Elution Buffer Volume / µL**	**Elution Temp. / °C**	**Number of washing steps**
1	150	100	25	2
2	15,000	40	42	2
3	15,000	40	25	3

Table 3.1.1 The elution conditions and cell numbers used in methods 1, 2 and 3 during protocol optimisation.

3.3 Spectrophotometric Analysis on the Nanodrop-1000

The Nanodrop-1000 pedestal was cleaned with molecular-grade water and KimWipes (KimTech Science, UK). 2 µL of Magsi-DNA Elution Buffer (blank) was used to initialize the reader and the settings set to read 'Nucleic Acids DNA'. 2µl of each sample (S1, S2 and S3) was pipetted onto the pedestal and the arm closed. The ratio of absorbance at 260 and 280 nm ($A_{260/280}$) was used to confirm the presence of DNA in the extracted solution, and the ratio of absorbance at 260 and 230 nm ($A_{260/230}$) was used to assess the purity of the DNA. An $A_{260/280}$ ratio of >1.8 is an acceptable indication of the presence of DNA and an $A_{260/230}$ of ~ 1.5 is accepted for "pure DNA". Using Beer's Law, the Nanodrop-1000 correlates absorbance at 260 nm with concentration of DNA in ng/µL. After each measurement, the pedestal was wiped with

a clean, dry KimWipe. The output of DNA was compared to the theoretical input and an average of percentage throughput was calculated for each sample (S1, S2 and S3).

3.4 Microfluidic Chip Fabrication

Microfluidic designs were made using SolidWorks software (Fig 3.3.1) and cut onto Red Self- Adhesive Vinyl paper (Vinyl Warehouse, UK) using a Graphtec Craft ROBO Pro S printer. The self-adhesive vinyl was then peeled off its sticky-back paper and fixed onto a petri dish, creating the master mold (Fig 3.3.2). To prepare the polydimethylsiloxane (PDMS), a SYLGARD® 184 Silicone Elastomer Kit was used.
30 g silicon elastomer was combined with 3 g crosslinker (curing agent) and this was mixed thoroughly for 5 minutes using a Pasteur pipette. Following this, the mixture was de-gassed under a vacuum for 10 minutes to remove air bubbles. The mixture was allowed to return to normal atmospheric pressure and the de-gassing procedure repeated until no bubbles remained. Following this, the mixture was poured over the master mould and allowed to cure overnight. To complete the curing process, the PDMS was peeled off the mould and left to dry at 100°C in the oven for an hour. The PDMS was then plasma-treated and sealed onto a glass side, creating an enclosed microfluidic chip.

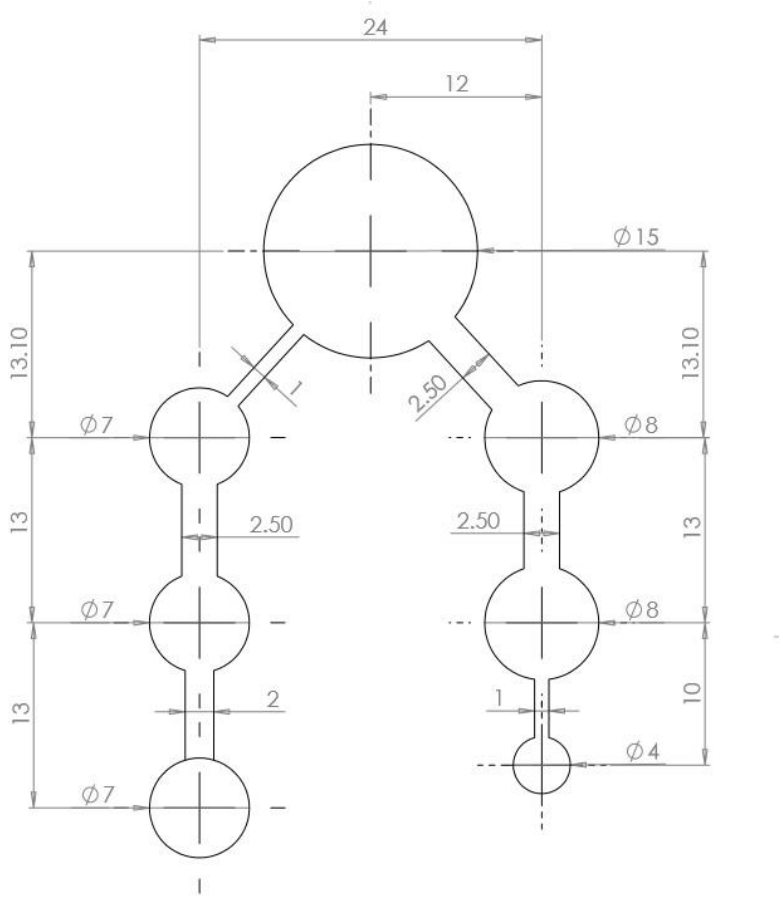

Fig 3.3.1 Microfluidic chip blueprint created on SolidWorks. All measurements shown are in mm.

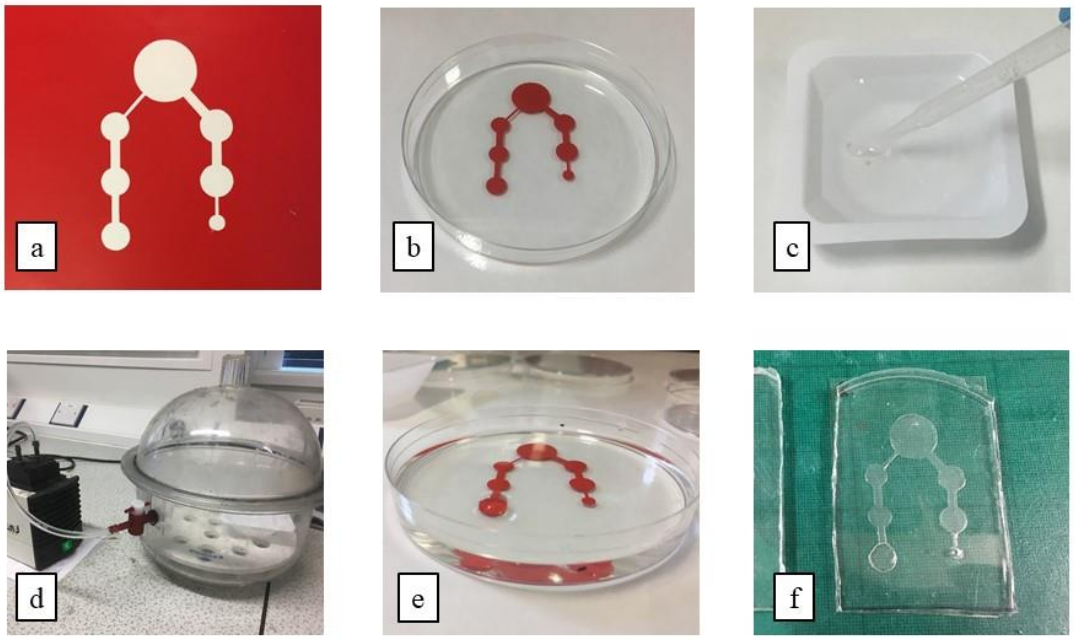

Fig 3.3.2 a) Blueprint printed onto adhesive vinyl, b) Master mould created on petri dish, c) PDMS and curing agent mixed manually, d) PDMS de-gassed and connected to vacuum pump, e) PDMS poured over mould and cured, and f) PDMS plasma treated before fixing onto glass slide.

3.5 PDMS Blister Fabrication

To drive the cell suspension and lysis buffer into the magnetic nanoparticle chamber, a finger-powered blister-switch was created using two methods. Firstly, a blister mould was designed on Solidworks software and 3D printed using an Ultimaker 2 Series 3D printer and secondly, cured PDMS was punched out into diameters of 7 mm to act as a mould. Both types of moulds were placed on the master mould created by the red adhesive vinyl paper in the petri dish and de-gassed PDMS poured over it. After curing, the PDMS was peeled off along with the embedded 3D printed and PDMS blisters (Figure 3.4.1).

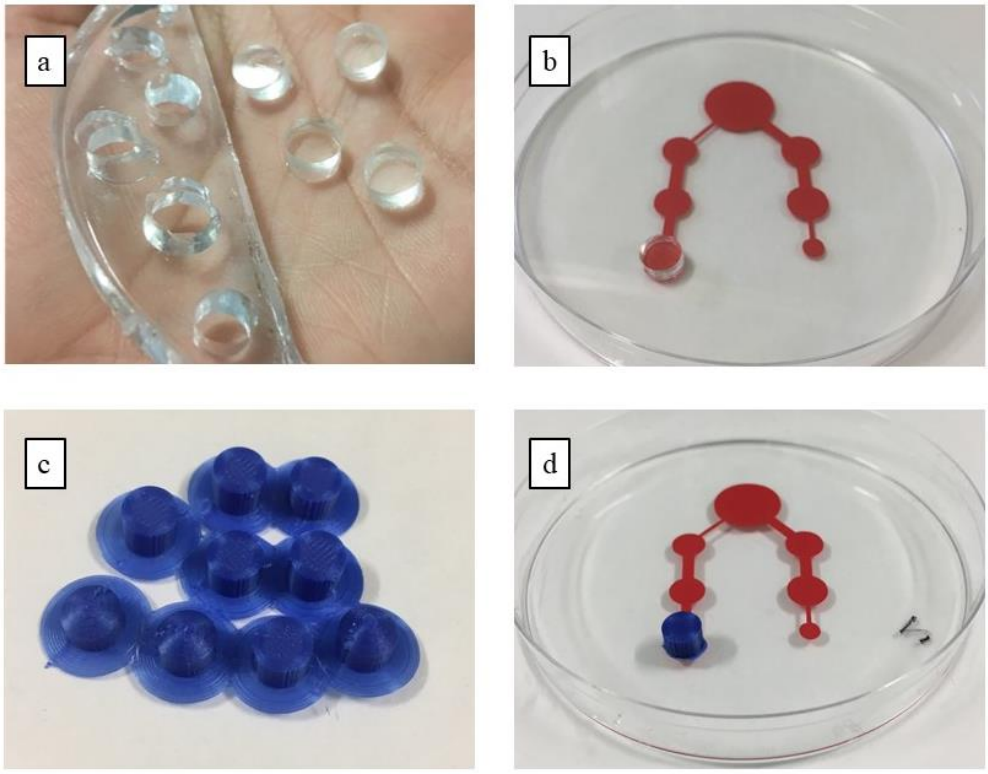

Figure 3.4.1 Blister moulds made of (a)(b) PDMS and (c)(d)3D printed plastic.

3.6 DNA Quantification per MG-63 cell

3.6.1 Approximation of DNA per MG-63 cell

For the purpose of this study, a theoretical value for the amount of DNA in an MG-63 cell was calculated as this is currently not reported in literature. The MG-63 cell line is a human cell line derived from the osteosarcoma of a 14-year-old male. A haploid human cell has a genome consisting of 3 billion base pairs. Each base pair has a molecular weight of 650 Daltons. To convert the haploid genome to diploid, a multiplication factor of 2 was applied. Using a conversion rate of 1 Dalton= 1.67×10^{-12} picograms, it was approximated that the DNA content per MG-63 is 6.513 picograms.

The calculation used was as follows:

$$\underbrace{3 \times 10^9}_{Base\ pairs} \times \underbrace{650}_{M_w} \times \underbrace{2}_{Diploid} \times \underbrace{1.67 \times 10^{-12}}_{Conversion\ to\ pg} = 6.513\ pg\ DNA\ per\ cell$$

Fig 3.6.1 Approximation of DNA in picograms per MG-63 cell.

For more information regarding this calculation and the haploid human genome, see *Appendix 1*.

3.6.2 PicoGreen Assay

MG-63 cells were seeded onto a 48 well-plate in increasing concentrations of 1000, 2000, 4000, 8000 and 10,000 cells/well in triplicate (n=3). Cells were incubated at 37°C and 10% CO_2 for 4 hours. Cell media was then removed from each well and cells washed twice with PBS. 150 µL CDB (Cell Digestion Buffer) was added to each well and incubated for 30 minutes. Following this, the well-plate was refrigerated at 4°C overnight. The next day, it was frozen at -80°C for 30 minutes and then thawed at 37°C for 30 minutes, completing one freeze-thaw cycle. This cycle was repeated twice, followed by the scraping each well's surface with a pipette tip, and the subsequent transferring of lysates into sterile 1.5 mL Eppendorf tubes.

Quant-it PicoGreen dsDNA Assay (ThermoFisher Scientific, UK) was used to quantify the amount of DNA in each MG-63 cell. An aqueous working solution of the PicoGreen dsDNA Quantitation Reagent was prepared by diluting the reagent 1:200 in 10 mM Tris-HCl and 1 mM EDTA solution (Tris-EDTA, pH 7.5). 100 µL PicoGreen reagent was added to 20.0 mL Tris-EDTA solution in a sterile plastic tube covered with foil. A five-point standard curve was created in triplicate (n=3) from 2000 to 10,000 cells.

Table 3.5.1 demonstrates the volumes of cell suspension. 90 µL PicoGreen solution was added to each well of a 96-well plate. Following this, 1.5 µL of the cell lysate was added to each well. The plate was left for 10 minutes at room temperature on a Stuart Gyrating Rocker, covered in foil, before measurement. After incubation, the sample fluorescence was measured using a fluorescence microplate reader (Tecan Infinite F200 Fluorescent Microplate Reader) at excitation of 480 nm and emission 520 nm. The fluorescence value of the reagent blank was subtracted from each of the samples to generate a standard curve of fluorescence against cell concentration.

Volume of 10,000 cells/mL stock solution (µL)	Volume of TE buffer (µL)	Volume of diluted PicoGreen reagent (µL)	Final conc. of cells in PicoGreen Assay (number of cells/µL)
1000	0	1000	10,000
800	200	1000	8,000
600	400	1000	6,000
400	600	1000	4,000
200	800	1000	2,000
0	1000	1000	Blank

Table 3.5.1 Volumes of cell suspension, TE buffer and PicoGreen reagent added for DNA Quantification Assay.

3.7 On-Chip DNA Extraction

All solutions were scaled down from the bench-top method by a factor of 40 based on the maximum volume of each chamber (Table 3.7.1).

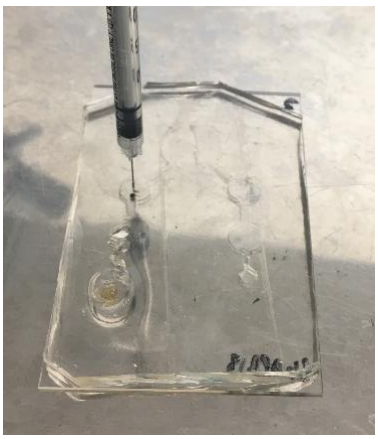

Fig 3.7.1 Injection of magnetic nanoparticles into the microfluidic device.

Sterile 0.3 mL Terumo® U-100 Insulin MyJector injections (Fig 3.7.1) were used to add all solutions into the chip. 5 µL MG-63 cell suspension in the concentration of 15,000 cells/µL was added to 3.75 µL lysis buffer in an Eppendorf tube outside the chip. This solution was vortexed and injected into the first chamber of the chip (Fig 3.7.2). The pressure-driven blister switch was pushed down using the index finger, which moved the cell lysate into the second chamber where 0.5 µL Magsi-DNA magnetic nanoparticles (MagnaMedics Diagnostics BV) were injected. The particles were collected using a neodymium magnet (Amazon,

UK) held under the chip, and brought into the third chamber where 11 µL binding buffer was added. The magnet was used to thoroughly mix the particles in the binding buffer, and then to bring them into the fourth chamber where 5 µL washing buffer-I was added for the purification process. Following this, the particles were brought into the fifth chamber where 5 µL washing buffer-II was added, and then finally, into the sixth chamber where 2.5 µL elution buffer was used to elute DNA off the particles. The eluted DNA was then collected from this chamber using a MyJector injection and transferred into a sterile Eppendorf tube. Following this, the sample was analysed on a Nanodrop-1000 Spectrophotometer.

Chamber	**Reagent**	**Bench-top volume / µL**	**On-chip volume / µL**	**Maximum volume of chamber / µL**
1	Cell suspension	200	5	10.78
	Lysis buffer	150	3.75	
2	Magnetic nanoparticles	20	0.5	10.78
3	Binding buffer	440	11	31.67
4	Wash buffer I	200	5	14.07
5	Wash buffer II	200	5	14.07
6	Elution buffer	100	2.5	3.52

Table 3.7.1 Maximum capacity of each chamber within the microfluidic chip and a comparison of volumes between bench-top and on-chip methods (scaled down by a factor of 40).

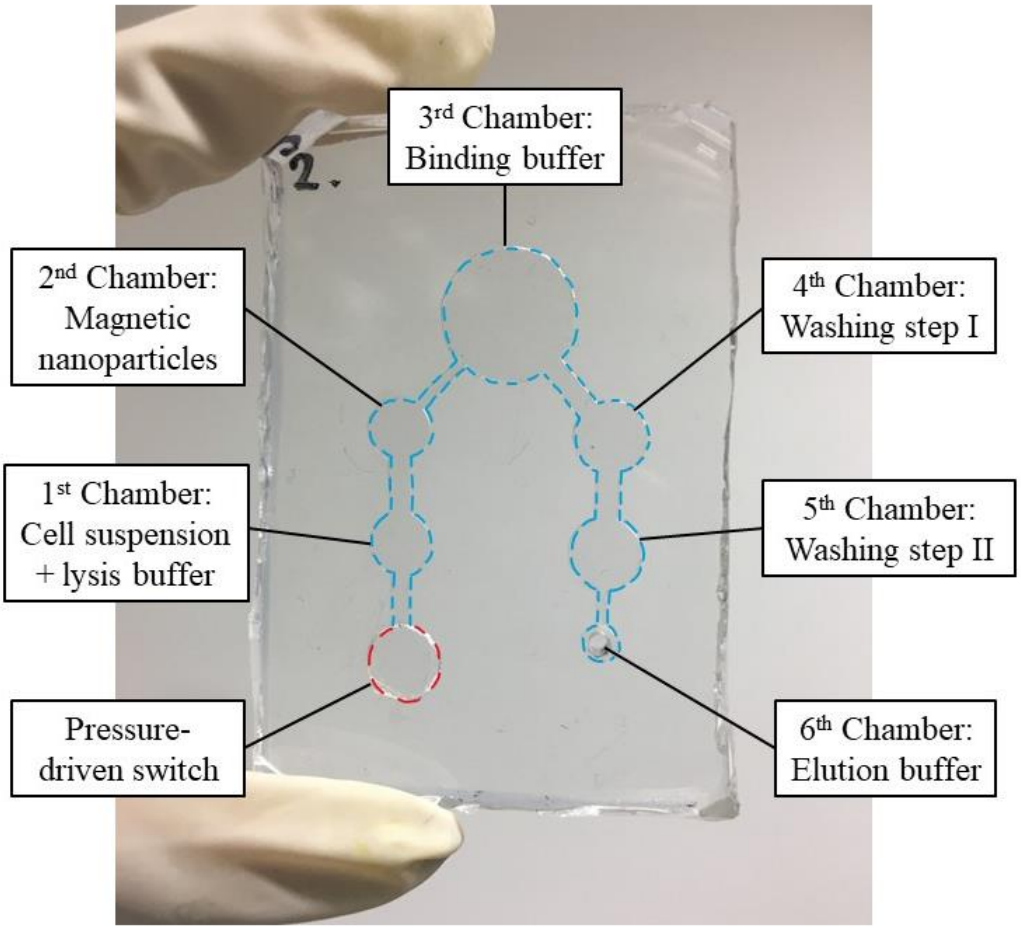

Fig 3.7.2 Prototype of microfluidic device for DNA extraction showing the sequence of steps starting with a blister which is pressed down to drive flow, followed by 1. Inlet for cell suspension or blood and lysis buffer, 2. Inlet for magnetic nanoparticles (MNPs), 3. Chamber for MNP-DNA binding, 4. And 5. Chambers for DNA purification, and 6. Chamber for elution off MNPs.

4. RESULTS

4.1 Bench-top Method

Percentage throughput was calculated to normalise the data obtained from methods 1, 2 and 3 (see Table 3.1.1) which, depending on the method, used different inputs of DNA (150 cells/µL for method 1 and 15,000 cells/µL for methods 2 and 3).

Percentage throughput is defined as the percentage of the theoretical input of DNA that successfully passes through the system and is extracted as the output. Equation 4.1.1 was used to calculate percentage throughput and the theoretical value used (6.513 pg/cell) was based on the calculation in Section 3.5.1.

Equation 4.1.1 $$Percentage\ throughput = \frac{Output\ of\ DNA}{Theoretical\ input\ of\ DNA} \times 100\%$$

where:

Equation 4.1.2 $$Output\ of\ DNA\ (ng) = Output\ DNA\ concentration\ (ng/\mu L) \times Elution\ volume\ (\mu L)$$

and:

Equation 4.1.3 $$Theoretical\ input\ of\ DNA\ (ng) = Total\ number\ of\ cells \times Theoretical\ value\ of\ DNA\ per\ cell\ (ng)$$

Figure 4.1.1 shows the percentage throughput for Samples 1, 2 and 3 across the three methods developed in the method optimisation process. Standard error (SE) was derived from the standard deviation (σ) and sample size (n) for each sample using the following equation:

Equation 4.1.4 $$SE = \frac{\sigma}{\sqrt{n}}$$

It can be seen that for Method 1, Samples 2 and 3 showed a significantly high percentage throughput (0.54% and 0.25%), whereas for Sample 3, a negative value is obtained (-0.014%). The large standard error seen in Sample 3 (0.475%) is derived from the variance seen across samples in Method 1.

For Method 2, Samples 1 and 2 (0.012% and 0.017%) are again significantly higher than Sample 3 (0.003%). For the same method, the standard error seen across Samples 1, 2 and 3 is relatively constant at 0.008%.

As for Method 3, it can be seen that Samples 1 and 2 have relatively similar percentage throughput (0.0022% and 0.0020%) whereas Sample 3 is slightly lower (0.001%). The standard error (0.0005%) seen across samples (S1, S2 and S3) in Method 3 stays relatively constant.

As for detecting the presence of DNA in Method 1, the $A_{260/280}$ ratios ranged from 2.0 to 2.95 which is greater than the accepted value for pure DNA (~1.8) [54]. To detect the purity of the extracted DNA, $A_{260/230}$ ratios were calculated which ranged from 0.02 to 0.04 for Method 1. This is much lower than the expected range for pure DNA (2.0-2.2). For Method 2, the $A_{260/280}$ ratios ranged from 1.94 to 3.78, and the $A_{260/230}$ ratios were slightly higher, ranging from 0.11 to 0.18. For Method 3, the $A_{260/280}$ ratios were much higher, ranging from 2.35 to 7.38, and the $A_{260/230}$ ratios were low as seen in Method 1, ranging from 0.01 to 0.03.

Method	**DNA presence / $A_{260/280}$**	**DNA purity / $A_{260/230}$**
1	2.26 ± 0.28	0.03 ± 0.009
2	2.52 ± 0.76	0.13 ± 0.76
3	4.07 ± 1.75	0.02 ± 0.009

Table 4.1.1Mean $A_{260/280}$ and $A_{260/230}$ ratios for bench-top Methods 1, 2 and 3.

Method optimization and variation between samples (S1, S2, S3)

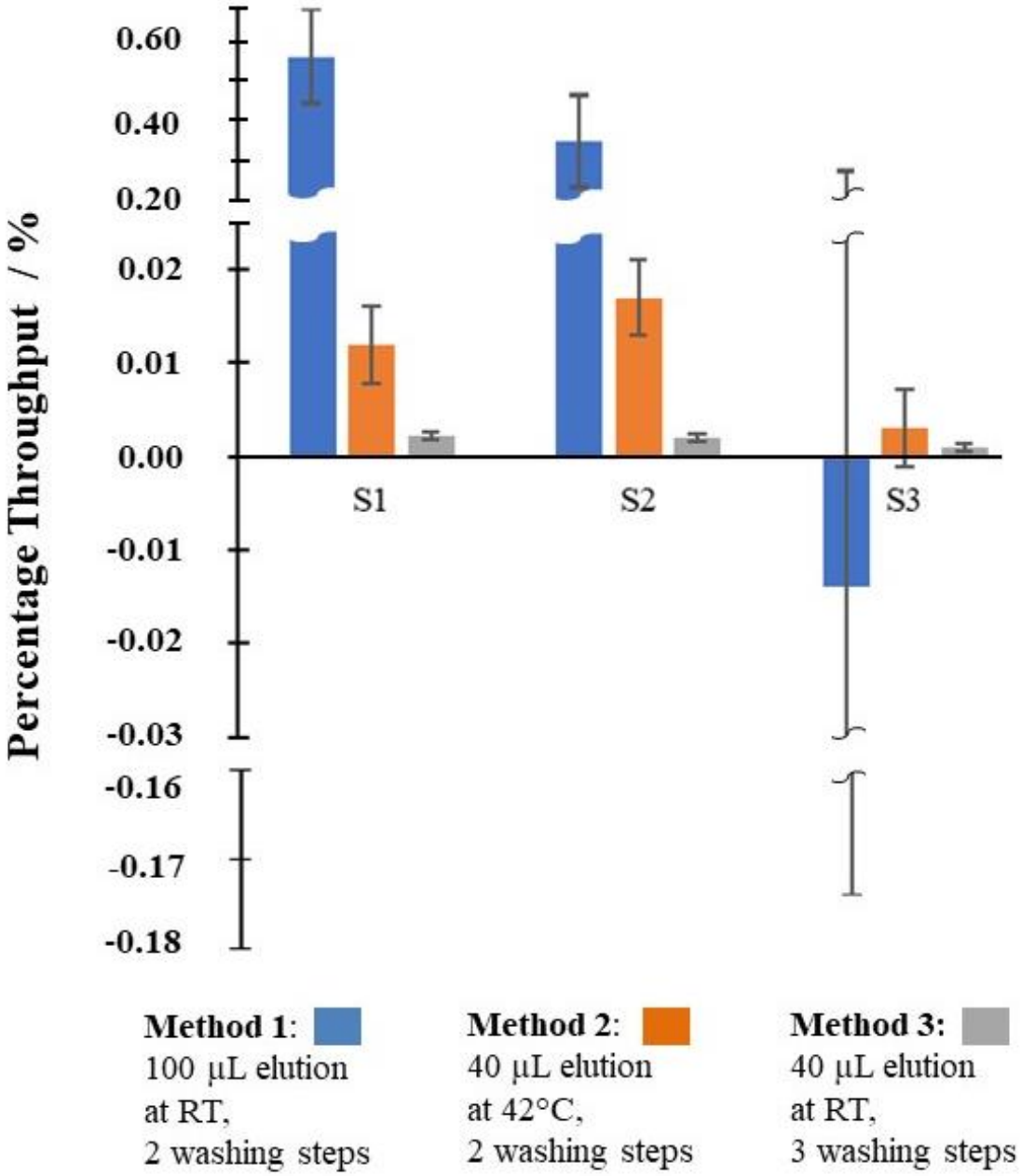

Fig 4.1.1 A comparison of percentage throughput of DNA between different versions in method optimisation. Standard error derived from SD.

Figure 4.1.2 shows the percentage throughput from six samples (S1-6) of calf thymus DNA at concentrations of 10 and 100 ng/µL. The percentage throughput for all samples at 10 ng/µL was negative with -34.9% mean percentage throughput and a standard deviation of 6.86%. The mean percentage throughput measured for the 100 ng/µL spiked solution was 20.8% with a standard deviation of 4.44%.

The $A_{260/280}$ ratios observed for the 100 ng/µL spiked solution were greater than 1.8, with a mean of 2.52 and standard deviation of 1.72 (*see Table 4.1.2*). The $A_{260/280}$ ratios observed for the 10 ng/µL spiked solution had a large range from -4.52 to 222.59, with a mean of 29.68 and a standard deviation of 95.57. $A_{260/230}$ ratios were negative at both concentrations, with a mean of -0.03 at 100 ng/µL and standard deviation 0.01, and a mean of at -3.00 at 10 ng/µL with a standard deviation of 1.47.

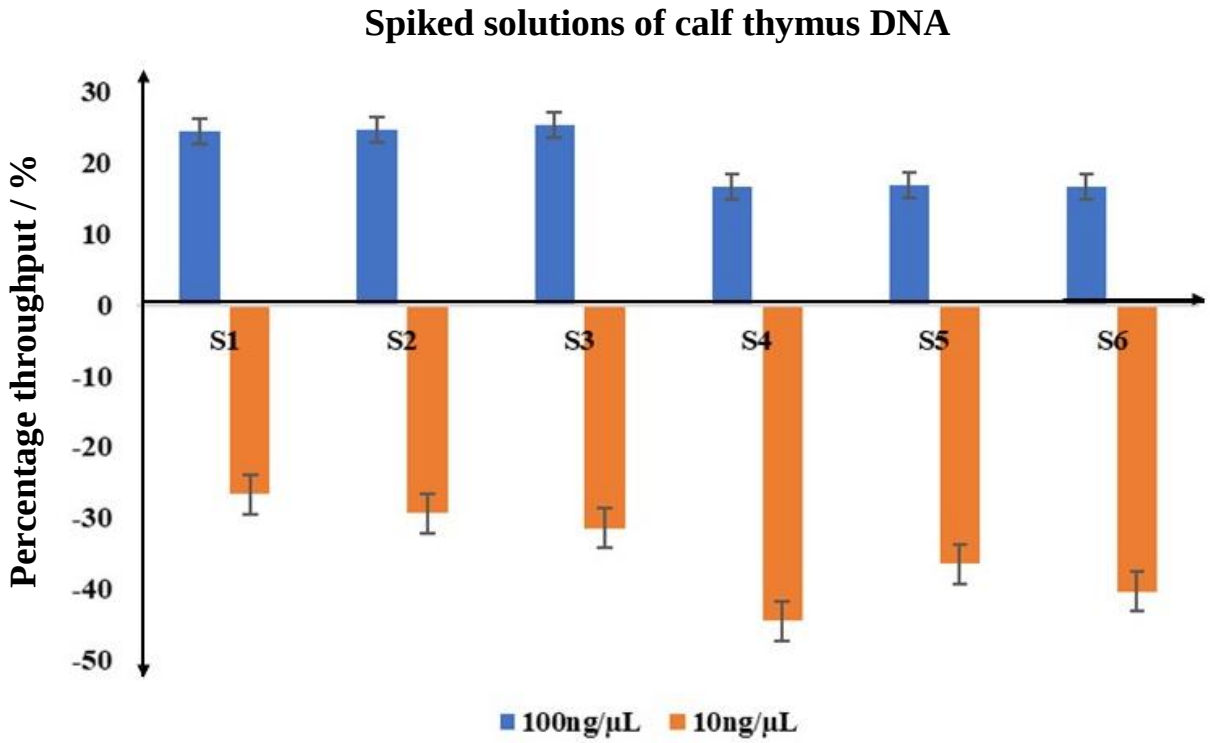

Figure 4.1.2 Percentage throughput measured using the Nanodrop for spiked DNA solutions at 100ng/µL and 10ng/µL with standard error derived from SD.

Concentration of DNA / ng/µL	DNA presence / $A_{260/280}$	DNA purity / $A_{260/230}$
10	29.69 ± 95.57	-0.03 ± 0.01
100	2.52 ± 1.72	-3.00 ± 1.47

Table 4.1.2Mean $A_{260/280}$ and $A_{260/230}$ ratios for bench-top extraction of calf thymus DNA.

4.2 On-chip Method

To compare DNA extraction between the bench-top and the chip, percentage throughput was plotted for both types of methods using MG-63 cells and calf-thymus DNA (Figure 4.2.1). As in the previous section, the input of DNA was based on the approximation of DNA content in an MG-63 cell (*see Section 3.5.1).* The concentration of the cell suspension was kept constant across both methods at 15,000 cells/µL.

The percentage throughput for MG-63 cells (20.6% ± 10%) was higher on the chip than that for calf thymus (9.7% ± 5%). Whereas on the bench, the opposite was seen; percentage throughput was higher for calf thymus (20.8% ± 5%) than for MG-63 cells (0.54% ± 10%).

To detect the presence of DNA and assess its purity, mean $A_{260/280}$ and $A_{260/230}$ ratios were determined. The mean $A_{260/280}$ ratio for MG-63 cells (6.09) on the chip was lower than that for calf thymus (11.50), both of which were higher than the accepted value of ~1.8 for pure DNA. The mean $A_{260/230}$ ratios for MG-63 cells (-0.41) and calf thymus (-1.47) were both negative on the chip, which was much lower than the accepted value for pure DNA (2.0-2.2).

The mean $A_{260/280}$ ratio for MG-63 cells (2.26) on the bench was lower than that for calf thymus (2.5), both of which were relatively close to the accepted value of ~1.8 for pure DNA. The mean $A_{260/230}$ ratio for MG-63 cells (0.03) on the bench was higher than that for calf thymus (-3.0) which was negative. Both values were significantly different from the accepted value for pure DNA (2.0-2.2).

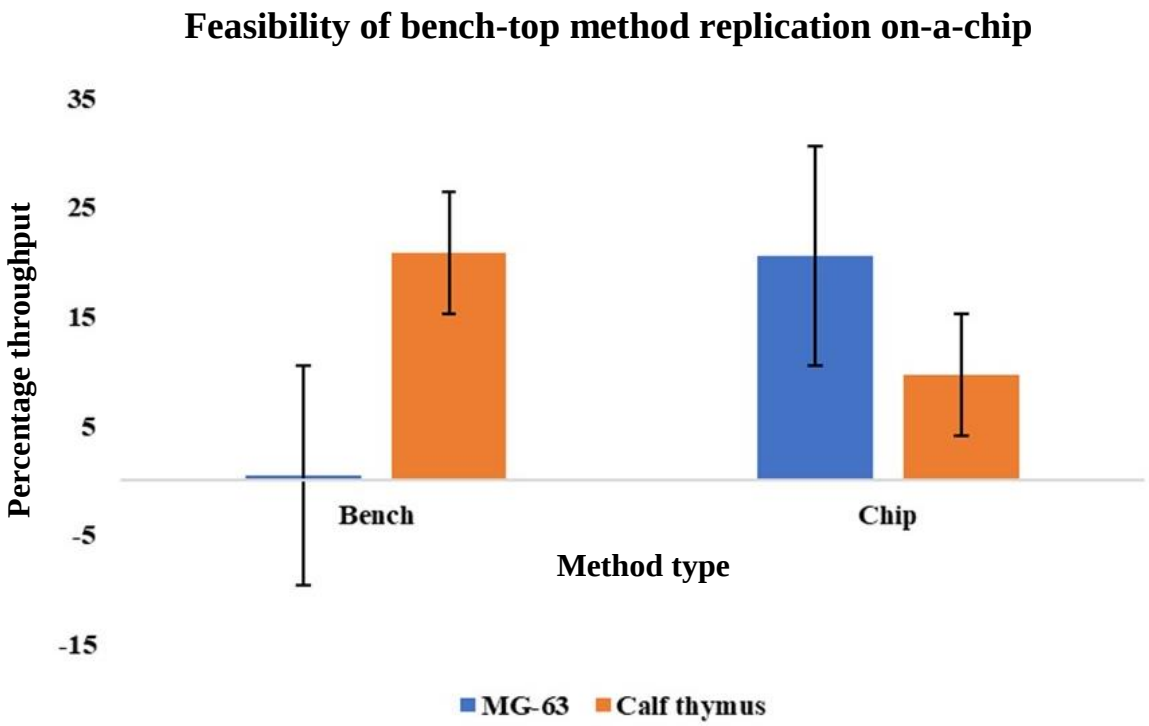

Fig 4.2.1 Percentage throughput of DNA using the bench-top method and the on-chip method (n=3). Error dervied from SD.

4.3 Microfluidic Chip Design

Microscopic images of the chips were taken after DNA extraction (Fig 4.3.1 and 4.3.2) to better understand the reasons behind low throughput. Fig 4.3.2a shows the leaking of magnetic nanoparticles (MNPs) out of channel boundaries and Fig 4.3.2c shows MNPs trapped between air bubbles within the fluid. Constricted channels were identified (Fig 4.3.2b) causing particles to be lost in carry-over between chambers (Fig4.3.2d).

Additionally, backflow of fluid was observed on release of the blister switch due to the build-up of negative pressure. Figure 4.3.3 shows the fluid meniscus between the first chamber and the blister switch, where MNPs are observed due to backflow.

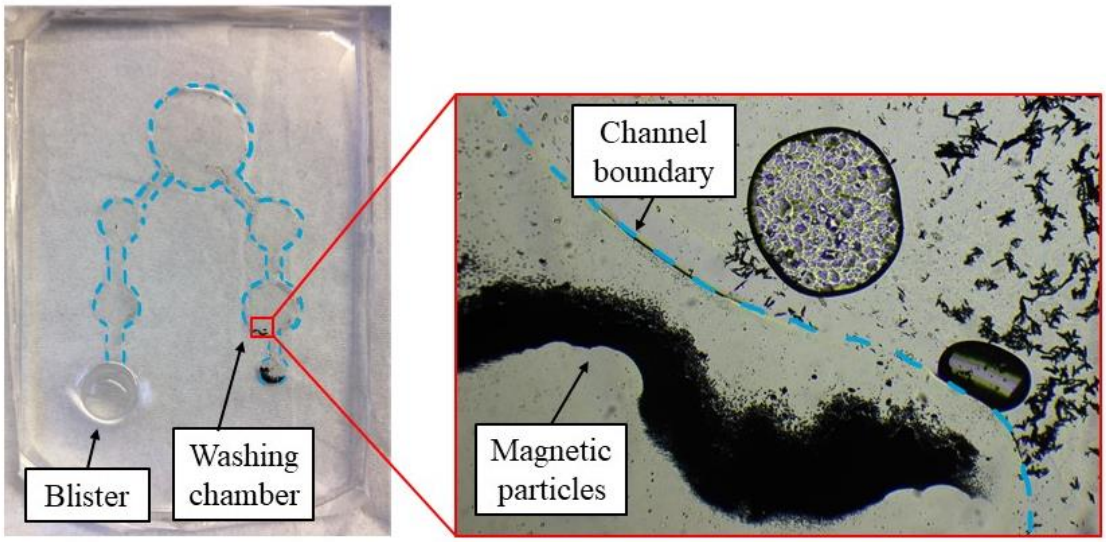

Fig 4.3.1 Collection of MNPs observed outside channel under the microscope after DNA extraction. Dotted lines represent channel boundaries (x20).

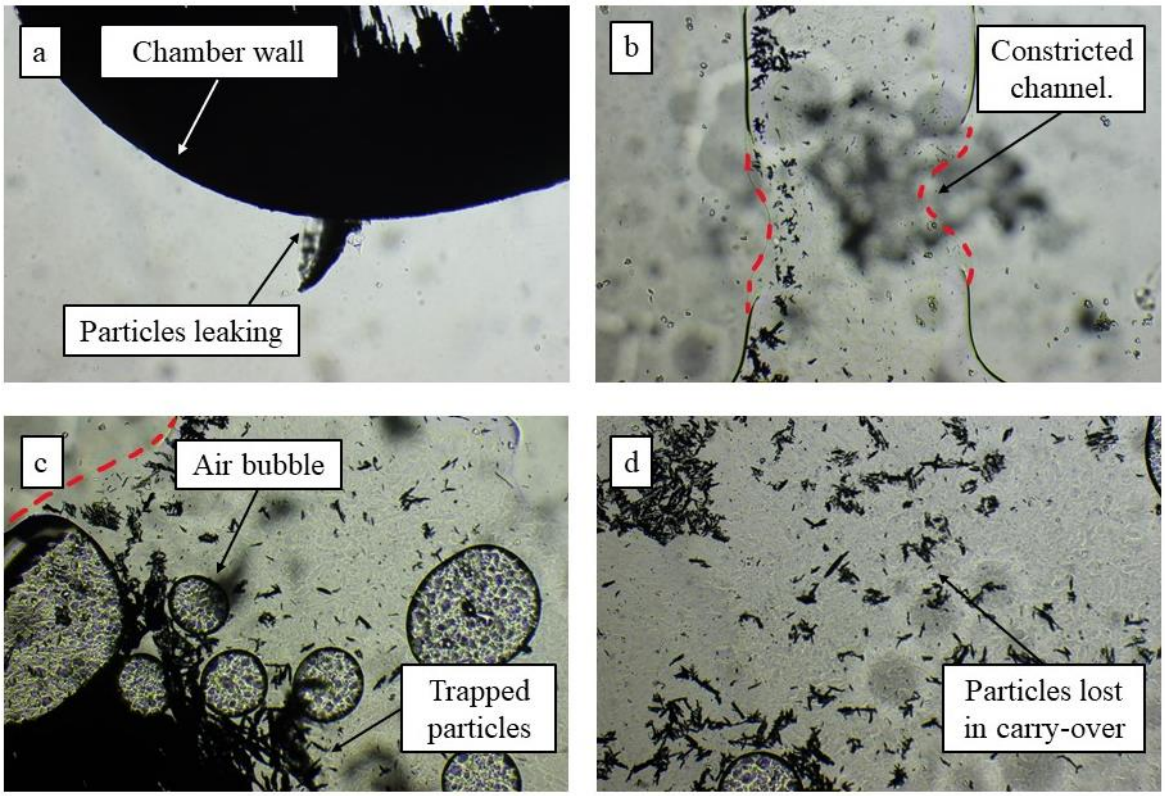

Figure 4.3.2 Loss of particles caused by the inaccuracies of the vinyl sticker-based fabrication method and mode of injection. (a) Particles moving out of a chamber, (b) collapsed channel, (c) air bubbles trapping particles and (d) particles lost in carry-over. Dotted lines represent channel boundaries.

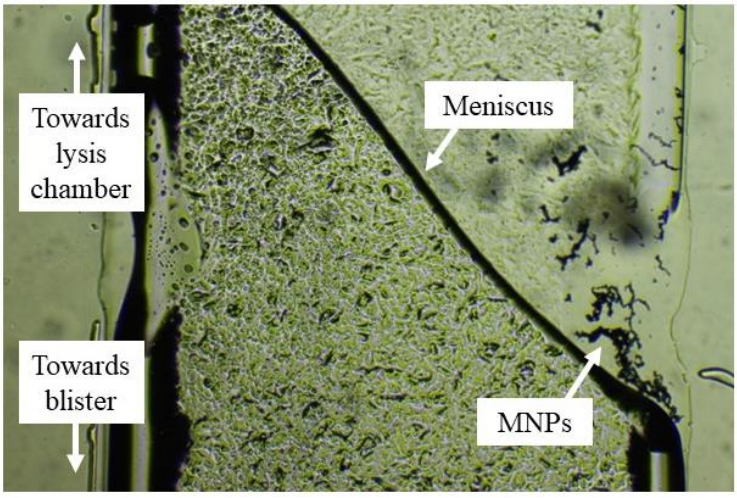

Figure 4.3.3 Magnetic nanoparticles carried away from the first chamber on release of the blister-switch.

4.4 PicoGreen DNA Quantification

To validate the theorised value of DNA in an MG-63 cell from Section 3.5.1, DNA was quantified using PicoGreen fluorescent dye and a standard curve relating fluorescence to the quantity of DNA was used to determine the amount of DNA in an MG-63 cell.

As seen in Figure 4.3.1, the absorbance values at 1,000 and 2,000 cells (4.67 AU) were the same. The absorbance value at 4,000 cells (23.67 AU) was higher than for 8,000 cells (14.67 AU) however, this picked up again at 10,000 cells (32 AU). The two anomalies observed at absorbance values of 2,000 and 8,000 cells, denoted as X_1 and X_2 in Figure 4.3.1, were ignored to avoid skewing in DNA quantification. As a result, the absorbance values at 1,000, 4,000 and 10,000 cells were plotted against DNA quantity (Fig 4.3.2), using a standard curve which relates the absorbance of light at 532 nm in PicoGreen dye to the quantity of DNA present in the solution [37].

The quantity of DNA observed per cell for 1,000 cells (7.292 pg) was lower than that observed for 4,000 cells (9.572 pg), whereas that observed for 10,000 cells (5.188 pg) was much lower than both. The mean value of DNA calculated from these three readings (1,000, 4,000 and 10,000 cells) was 7.350 pg per cell which is slightly higher than the theorised value of 6.513 pg per cell.

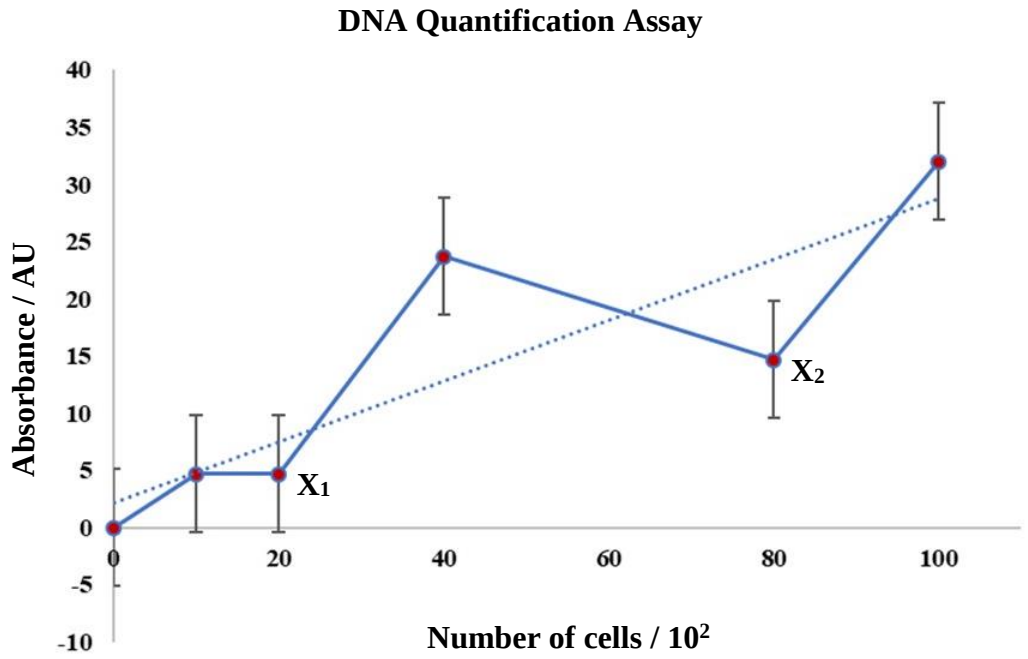

Fig 4.3.1 Results of PicoGreen Assay of MG-63 cells seeded at 1000, 2000, 4000, 8000 and 10,000 cells/well in triplicate (n=3). Anomalies shown at cell seeding densities X_1 = 2,000 and X_2 = 8,000.

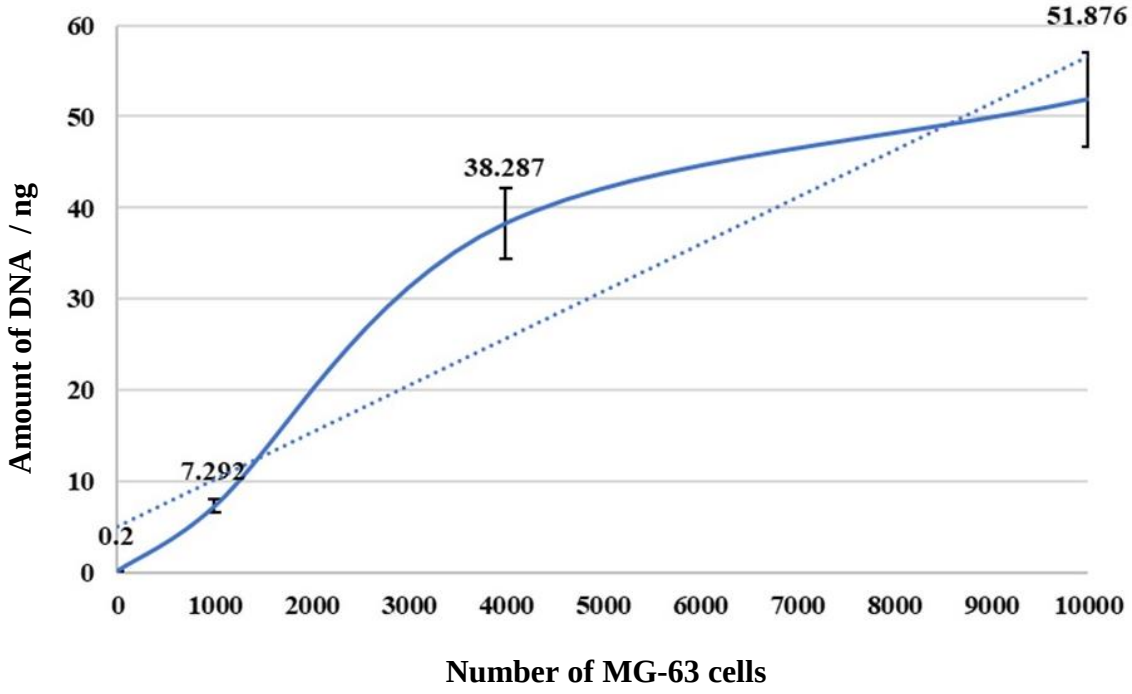

Standard curve derived from data in the study by Serth et. al [38].

4.5 Summary of Results

DNA was extracted from MG-63 cells at a low throughput of 0.54% on the bench. Bench-top DNA extraction resulted in a higher yield of DNA (9.7%) for the spiked solution, however, MG-63 cells showed a higher throughput on the chip (20.6%). DNA extraction was replicated on a microfluidic chip with six chambers for lysis, mixing with MNPs, binding, washing off impurities and elution. A blister-driven switch was added to the chip to push the cell lysate into the MNP chamber. From here on, a magnet was used to drive flow. A theoretical value of 6.513 pg DNA was calculated per MG-63 cell, and this was validated against a standard curve (O'Neill et. al) to give 7.350 pg per cell.

Out of these, method 1 had the highest percentage throughput at 0.54% whereas methods 2 and 3 were lower at 0.017% and 0.0022% respectively.

Despite multiple efforts to optimise the DNA extraction protocol on the bench – through increasing cell concentration and elution temperature, reducing elution volume and spiking the solution with calf thymus DNA – optimisation was not successfully achieved; however, higher reliability of results was obtained.

5. DISCUSSION

5.1 Optimisation of Bench-top Method

The large variance observed between samples of Method 1 (Fig 4.1.1) and the negative result of Sample 3 (-0.014%) can be attributed to the non-homogenous mixing of the cell solution prior to aliquoting cells. As anything in suspension of higher molecular weight sinks to the bottom of the tube, non-homogenous mixtures are easily developed in procedures with several steps such as DNA extraction. Bienvenue et. al studied different mixing techniques in homogenizing solutions of sperm cells before DNA extraction for forensic analysis [55]. This study observed that manual agitation and inversion techniques led to large deviations (average = 111 ± 53 cells/mL) between aliquoted cell solutions, whereas high-speed vortexing every 10-15s led to significantly more homogenous aliquots (average = 90 ± 3 cells/mL) [39]. Mixing via pipette is a form of manual agitation which may not have effectively homogenised cell solutions in this study, leading to large variances between samples across Method 1 (0.475% standard error). Additionally, vigorous mixing by pipette can instil air bubbles, creating froth within the solution which has shown to trap cells and DNA within the liquid menisci of bubbles [40] [41]. This is an even greater problem when working with volumes at the µ-scale as froth can take up a significant volume of the solution, as shown in Fig 5.1.1.

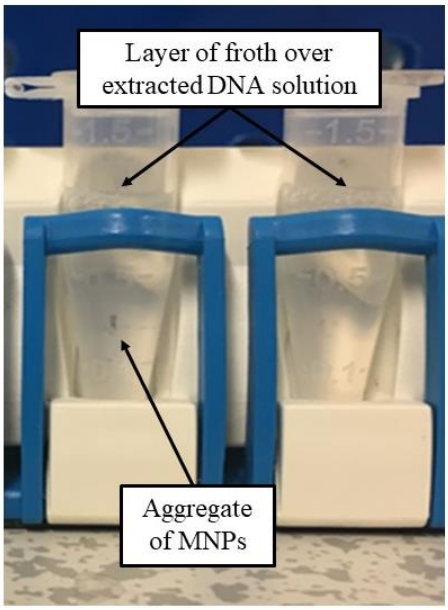

Figure 5.1.1 Froth developed through vigorous mixing using a pipette.

Because of non-homogenous mixing and the loss of DNA through bubbles, there may not have been sufficient DNA to detect in Sample 3 of Method 1, such that the DNA concentration may have been lower than the detection limit of the Nanodrop (2 ng/µL), thus giving an unreliable result of -0.014%.

Additionally, the relatively high percentage throughput seen in samples 1 and 2 of Method 1 (0.54% and 0.25%) in comparison, could have been overestimated due to the presence of other molecules that absorb at 260 nm, such as RNA from cell lysate [37]. The Nanodrop spectrophotometer uses Beer's Law (Equation 2.2) to quantify DNA concentration from the level of absorbance seen at 260 nm (A_{260}) [57]. As a non-specific method, spectrophotometric analysis will pick up any molecule that absorbs light at this wavelength and mask RNA as DNA. An overestimated A_{260} value will lead to high $A_{260/280}$ ratios, as seen for all samples (S1, S2 and S3) across all methods (1, 2 and 3). Alternatively, proteins may balance out some of the overestimation seen in $A_{260/280}$ ratios by contributing to the absorbance at 280 nm (A_{280}). Fig 5.1.2 shows an absorbance spectrum of DNA and BSA (Bovine Serum Albumin), a type of protein found in cows, demonstrating that a peak at 280 nm caused by proteins can be a source of error in absorbance ratios. Fluorescent dyes – such as PicoGreen and SYBR Green I – are more accurate in detecting DNA in the presence of impurities such as RNA and proteins. The only limitation with these dyes is their high cost which prevents them from being deployed for diagnostic screening in developing countries.

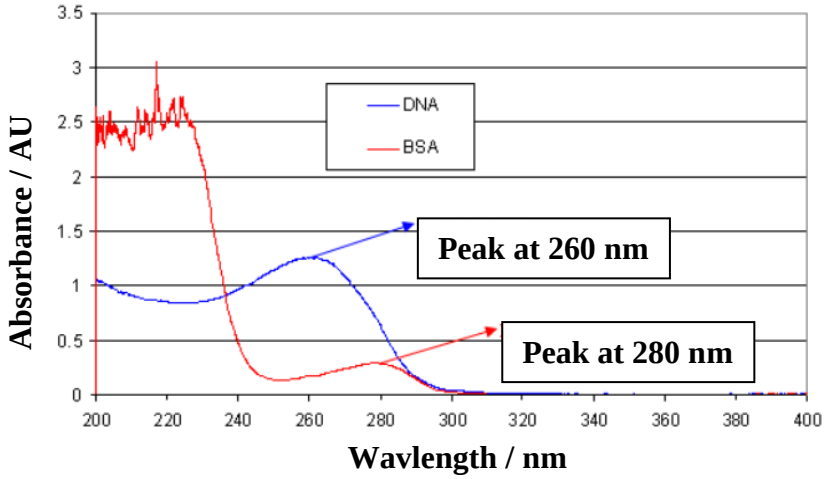

Fig 5.1.2 Absorbance spectra of DNA and proteins (BSA) at 260 and 280 nm (O'Neill et. al, 2011 [37]).

As the percentage throughput decreased quite significantly from Method 1 to 3 (0.54% to 0.0022%), the objective of optimising the DNA extraction method on the bench top was not met. However, standard error was reduced from 0.475% in Method 1 to 0.0008% in Method 3, resulting in an increase of the reliability of the method. As DNA extraction relies quite heavily on laboratory skills, standard error may have seen a decrease due to practice with the method over time.

Additionally, the concentration of cells was increased by a factor of 100 (*see Table 3.1.1*) when moving from Method 1 (150 cells/µL) to Method 2 (15,000 cells/µL). To portray the concentration of white blood cells in whole blood (4,000-10,000 cells/µL) and neglect the effects of non-homogenous mixing [42], a concentration of 15,000 cells/µL was chosen. However, through the results obtained, it is observed that an increase in cell concentration did not result in a proportional increase in DNA extraction which indicates that cells were not completely lysed. In a study testing the efficiency of bacterial cell lysis of M. smegmatis [43], efficiency was calculated based on the release of total DNA content. An extraction efficiency of 4.0% was observed when bacteria were exposed to water at 100°C for 10 mins and 6.6% on heating with Triton-X. On addition of guanidine hydrochloride to the Triton-X solution, a chaotropic salt used in commercial lysis buffers such as MagnaMedic's, extraction efficiency increased to 7.0%. In comparison to this study, extraction efficiency (also defined as *percentage throughput*) observed for MG-63 cells (0.54%) was much lower than expected. It is also worth noting that procedural errors may have occurred from the manual counting of cells where studies in the past have shown technicians performing duplicate cell counts, which means that the actual concentration of cells in solution is less than expected [44].

Non-specific absorbance is observed at 230 nm by buffer salts left-over from lysis, binding, washing and elution buffers, which could be a reason behind the low $A_{260/230}$ ratios observed for samples across all methods [37]. To overcome this, Method 3 incorporated an additional washing step with wash buffer-I to further purify DNA. However, since Method 3 had the lowest $A_{260/230}$ ratio (0.02% ± 0.009%) as compared to Method 1 (0.02% ± 0.009%) and 2 (0.13% ± 0.76%), it was concluded that the washing step was not effective in removing impurities as desired. Since the magnetic extraction protocol relies heavily on good pipetting technique, and the complete

removal of supernatants containing salts, some error may have been induced due to the challenges seen with complete removal of supernatants without disturbing the magnetic beads, especially at volumes of less than 100 µL.

While the effects of reducing elution buffer volume from Method 1 (100 µL) to Method 2 (40 µL) – in an attempt to concentrate the extracted DNA by a factor of 5 from 200 µL cell suspension – did not increase throughput, Method 2 showed less variance (0.017% ± 0.008%) between samples S1, S2 and S3, as compared to Method 1 (0.54% ± 0.475%). The low percentage throughput of S3 from Method 2 may have come from the incomplete incubation of the sample at 42°C. Although time was kept using a stopwatch, there may have been small discrepancies between the incubation times of the samples due to the limitation of only being able to treat one sample at a time.

The negative percentage throughput (-34.9%) obtained for the 10 ng/µL spiked solution is not surprising because of the lower detection limit of the Nanodrop-1000 Spectrophotometer (2 ng/µL). If coupled with the standard error (± 6.86 %) caused by the non-homogenous mixing of DNA prior to aliquoting, it could mean that the actual concentration of the 10 ng/µL solution is less than 2 ng/µL. This is confirmed by the positive percentage throughput (20.8%) seen for all samples (S1-6) of the 100 ng/µL spiked solution. Additionally, the negative $A_{260/230}$ ratios observed at both concentrations (10 and 100 ng/µL) may have been caused by the contamination of the blank solution used to initialise the Nanodrop. If the blank measurement has a higher absorbance reading at 230 nm than the spiked samples, then this will cause negative A_{230} ratios to develop once the blank is subtracted from sample readings. As discussed previously, the contamination at 230 nm comes from guanidine-derived chaotropic salts found in the buffers of commercial DNA extraction kits, which contribute to a peak near 230 nm [45]. Since spiked solutions were pure calf thymus DNA, it is unlikely that RNA which absorbs at 260 nm, would be present in the sample from the external environment. Additionally, the $A_{260/280}$ ratios are positive at both concentrations which eliminates the risk of contamination coming from proteins at 280 nm. In conclusion, it can be confirmed that the contamination occurred at 230 nm, creating higher A_{230} values for the blank measurement and inherently resulting in negative $A_{260/230}$ ratios at both concentrations.

The spiked solution of calf thymus indicates an inherent variability between $A_{260/280}$ ratios and that this is greater than 1.8 for pure DNA, validating the other absorbance results produced in this study.

5.2 Feasibility of Replication on a Microfluidic Chip

MG-63 cells had a higher percentage throughput on the chips (20.8%) as compared to on the bench (0.54%). While this was unexpected, it is worth noting that chip-based results in this study are associated with greater error and the likelihood of overestimation since a blank reading was not subtracted from absorbance measurements at 260 nm. While subtracting a blank reading is good practice, it could not be carried out due to the nature of the chips being one-time-use only. Calf thymus DNA showed more realistic results where throughput on the bench (20.6%) was more than double that on the chip (9.7%), however, percentage throughput on the chip is also associated with error due to the lack of blank reading subtraction.

While both MG-63 and calf thymus results show that it is feasible to replicate the bench-top DNA extraction method on a chip, it highlights the need for the further optimisation to achieve better percentage throughput and more reliable results.

Surprisingly, the throughput of MG-63 cells (20.8% ± 10%) achieved on the chip is higher than that achieved by calf thymus DNA (9.7% ± 5%). Typically, pure DNA without impurities from the cell lysate, produces greater throughput in extraction systems as there is less interference from circulating proteins and RNA molecules. Therefore, RNA would have contributed to the overestimated throughput in MG-63 DNA extraction on the chip where volumes were scaled down by a factor of 40 to fit within the maximum capacity of each chamber (*see Table 3.7.1)*. The accuracy and reproducibility of volume addition to the chip were limited by the 0.3 mL insulin injections (*Figure 3.7.1*). It was particularly challenging to prevent air bubbles when ejecting volumes due to the large injection forces exerted. This caused some solutions to overflow or be forced out of chamber walls, particularly during the addition of the 0.5 µL magnetic nanoparticles (*Figure 4.3.2c*). Additionally, it was found that a minimum of 30 µL elution buffer is required for the efficient elution of DNA from the

MNPs (based on manufacturer's instructions, *MagnaMedics Diagnostics BV*), however, the maximum capacity of the elution chamber in the current device is only 3.52 µL (*See Table 3.7.1*) of which 2.5 µL was added to prevent overflow. This may have been a limitation in achieving a better throughput on the chip and points to the need for larger chambers or microfluidic reservoirs. Despite the benefits of scaling down reaction volumes in microfluidics, such as greater sensitivity, less risk of contamination, lower cost and greater throughput [24], a disadvantage that is often overlooked at the µ-scale is the faster reaction time, as a result of which reactions may not achieve completion which would explain why a lower percentage throughput was observed for calf thymus DNA on the chip than on the bench.

Another contributing factor to lower throughput on the chip was the particle retention observed between chambers (*see Figures 4.3.1, 4.3.2 and 4.3.3*) which suggests that the positively charged silica-coated MNPs are attracted to the negatively charged PDMS [46], causing DNA-bound to the particles to be lost in transit. While oxygen plasma treatment – as conducted to bond the PDMS onto the glass slide in Section 3.4.1 – attaches silanol (SiOH) groups to the surface of PDMS, these groups are short-lived and the surface soon reverts to its native state within 2 hours [47]. Alternatively, PDMS can be coated with PEG (polyethylene glycol) brushes that help increase the hydrophilicity of the surface and overcome particle retention [47] [48].

However, there are some limitations in increasing throughput such as the low manufacturing reproducibility of the microfluidic chips, which points to the need for more sophisticated methods of microfabrication and an embedded amplification system such as RT-LAMP (Reverse Transcriptase Loop-mediated Isothermal Amplification).

Additionally, backflow of liquid was created on release of the blister due to negative pressure build-up which caused loss of particles (*Figure 4.3.3*). However, this was overcome by punching a hole in the PDMS between the blister and the first chamber which was then used to relieve negative pressure and successfully prevent backflow.

5.3 DNA Quantification

The C-value is defined as the amount of DNA in picograms present within a haploid human nucleus. The C-value is dependent on a variety of factors such as polymorphism and the number of base pairs (bp) within the haploid genome. Each of the four base pairs – adenine, guanine, cytosine and thymine – have a slightly different weight due to the variable regions found on the bp. Serth et. al reported a value of 6.57 pg for the diploid genome after conducting DNA extraction from renal cancer and prostate hyperplasia cells and quantitating them with PicoGreen [38]. Morton et. al reported a similar C-value of 3.5 pg for the haploid nucleus, doubling which gives us 7.0 pg per diploid cell [49]. These values are extremely close to the theoretical value achieved in this study (6.513 pg) where the C-value would equal half that approximated, i.e. 3.315 pg.

Additionally, Serth et. al concluded that PicoGreen was an accurate method of DNA quantitation with the lowest threshold for DNA detection at 120 diploid cells [38]. This is far from the lowest threshold offered by spectrophotometry, which was 30,000 diploid cells in this study. *Fig 5.4.1* shows a standard curve relating absorbance to DNA quantity in ng, derived using PicoGreen analysis in the study by Serth et. al [38]. This curve was used to quantitate DNA from absorbance readings produced in *Section 3.4.1,* and to validate the hypothesis that there is approximately 6.513 pg DNA in an MG-63 cell. The value of DNA calculated from this standard curve was 7.350 ± 1.27 pg per cell. The small difference seen between these two values suggests that the theoretical DNA input used for the calculation of percentage throughput values is relatively reliable.

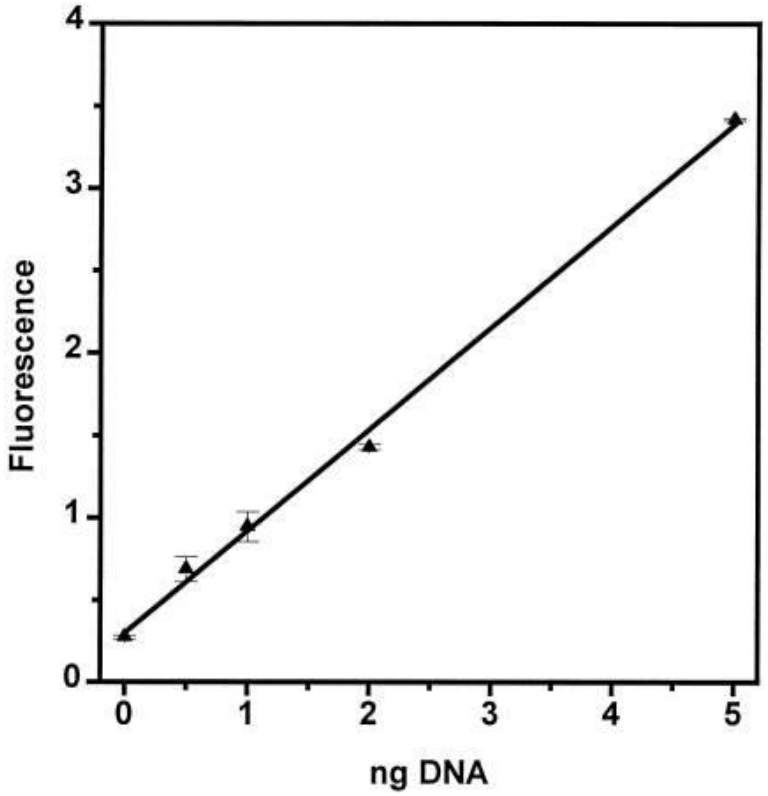

DNA standard curve by Serth et. al. Linear regression applied [38].

5.4 Summary of Key Findings

Significant loss of DNA occurred through combined sources of error, such as incomplete cell lysis, non-homogeneity of samples, loss of particles in carry-over and the presence of RNA, protein and buffer salts in solution. The bench-top DNA extraction method was attempted to be optimised, however, this not produce successful results. The bench-top method was however, successfully scaled down to work at the µ-scale. A prototype of the microfluidic device was fabricated, showing comparable results for the spiked solutions of DNA between the bench and the chip. A blister-switch and pressure-release nozzle was incorporated within this device to drive flow and relieve the negative pressure created.

5.5 Limitations and Future Development

All percentage throughput values are limited by the theoretical value of DNA in MG-63 cells that is based on the number of base pairs in the haploid human genome. Despite having conducted the PicoGreen assay and validated this against a standard curve created by Serth et. al, there is still some degree of error associated with using a standard curve made under different laboratory conditions. For more reliable results, a standard curve should be created alongside test readings to ensure reproducibility. Additionally, all chip-based measurements of percentage throughput are overestimated due to the lack of a blank. The reliability of these results is therefore limited and this needs to be re-conducted with a blank chip to validate obtained results.

While the MG-63 cell line formed a good DNA model for the creation of a prototype in this study, a more representative model of white blood cells should be used in the future for the intended diagnostic application. The K-562 or the RS4;11 cell lines could be used for future development, both of which are both lymphoblast cell lines derived from leukemia in the bone marrow, or the CA46 cell line, which is a B-lymphocyte derived from Burkitt's lymphoma [50] [51] [52]. Using cell morphology as similar in representation to white blood cells (WBCs) will allow the DNA extraction method to be optimised for extraction of DENV (Dengue Virus) from WBCs.

As for developing the microfluidic design, there is a need for a more autonomous system as opposed to a chip that requires subsequent injection of each buffer, especially as difficulty was faced when injecting samples into chambers. To overcome this, future versions of the chip could look at incorporating retention burst valves (RBVs) and trigger valves (TVs) as presented by Safavieh et. al [30]. While a future development of this device could explore the conjugation of polyethylene glycol (PEG) brushes onto the PDMS surface to prevent particle retention, another development could be to replace PDMS with the Flexdym elastomer [53]. Flexdym offers advanced hydrophilization and bonding performance in microfluidic devices with a faster microfabrication process, that has not yet been achieved through other materials such as micro-milling, 3D printing or paper-based microfluidic technologies.

Since it was found that non-specific absorption in spectrophotometry induces inaccuracies in output measurements, particularly for impure DNA, future development of this method should explore other low-cost read-out methods such as PCR (Polymerase Chain Reaction).

In the long-term, DENV-specific aptamers could be used to increase the sensitivity of the device and RT-LAMP could be used to amplify the RNA. Moreover, the development of this assay should move into the expected concentration range seen for the Dengue Virus (DENV) in patients (0.32–267,516 PFU eq/mL for DENV-1 infections and 0.30–124,097 PFU eq/mL for DENV-2 infections) so that the required sensitivity is achieved through optimisation [31].

6. CONCLUSION

This study reports a prototype of a microfluidic device for the magnetic extraction of DNA from MG-63 cells. Silica-coated magnetic nanoparticles (MNPs) were used to separate DNA from cell lysate in the presence of chaotropic salts. Optimisation was attempted for the bench-top extraction method, however, was unsuccessful in increasing percentage throughput. The bench-top method was scaled down onto a lab-on-a-chip device, utilising 40X times less reagent than on the bench. The microfluidic device performed the functions of cell lysis, MNP mixing, binding, washing and eluting DNA. A theoretical value of DNA content in MG-63 cells (6.513 pg) was proposed which was validated against results obtained from the PicoGreen assay (7.350 pg). Percentage throughput of MG-63 cells on the bench was 0.54% and on the chip was 20.6%, both with significant error of ± 10%. The limit of detection observed in this study was 100 ng/µL DNA on the bench. Future development of this device should include testing DNA extraction with a more representative model of white blood cells such as the K-562, RS4;11 or the CA46 cell lines, and coating the PDMS surface of the chip with PEG (polyethylene glycol) to reduce particle absorption.

7. REFERENCES

[1] R. W. Peeling et al., "Evaluation of diagnostic tests: Dengue," Nat. Rev. Microbiol., vol. 8, no. 12, pp. S30–S38, 2010.

[2] J. M. Heilman, J. De Wolff, G. M. Beards, and B. J. Basden, "Dengue fever: A Wikipedia clinical review," Open Med., vol. 8, no. 4, pp. e105–e115, 2014.

[3] E. Widajanti, H. Garna, A. Chairulfatah, and D. Hudaya, "Paediatrica Indonesiana," *Paediatr. Indones.*, vol. 49, no. 6, pp. 158–161, 2003.

[4] P. Yager, G. J. Domingo, and J. Gerdes, "Point-of-Care Diagnostics for Global Health," Annu. Rev. Biomed. Eng., vol. 10, no. 1, pp. 107–144, 2008.

[5] Iron Oxide Nanoparticles - Nanomaterials," Sigma-Aldrich. [Online]. Available: https://www.sigmaaldrich.com/materials-science/material-science-products.html?TablePage=119470654. [Accessed: 25-Apr-2018].

[6] L. de Bruin, "MagSi-DNA," *MagnaMedics*. [Online]. Available: http://www.magnamedics.com/index.php/magsi-dna. [Accessed: 25-Apr-2018].

[7] Kapelan Media, "SiMAG - affinity," *SIMAG Affinity : Magnetic nano and micro particles by chemicell*, 06-Jan-2007. [Online]. Available: http://www.chemicell.com/products/microparticles/simag-affinity/index.html. [Accessed: 25-Apr-2018].

[8] S. C. Tan and B. C. Yiap, "DNA, RNA, and protein extraction: The past and the present," *J. Biomed. Biotechnol.*, vol. 2009, 2009.

[9] R. Dahm, "Discovering DNA: Friedrich Miescher and the early years of nucleic acid research," *Hum. Genet.*, vol. 122, no. 6, pp. 565–581, 2008.

[10] M. B. Johns and J. E. Paulus-Thomas, “Purification of human genomic DNA from whole blood using sodium perchlorate in place of phenol.,” *Anal. Biochem.*, vol. 180, no. 2, pp. 276–8, 1989.

[11] “Phenol/chloroform extraction,” *Phenol/chloroform extraction - OpenWetWare*. [Online]. Available: https://openwetware.org/wiki/Phenol/chloroform_extraction. [Accessed: 29-Apr-2018].

[12] “Dynabeads™ MyOne™ Silane,” *Dynabeads MyOne Silane - Thermo Fisher Scientific*. [Online]. Available: https://www.thermofisher.com/order/catalog/product/37002D?SID=srch-srp-37002D. [Accessed: 29-Apr-2018].

[13] L. de Bruin, “MagSi-DNA,” *MagnaMedics*. [Online]. Available: http://www.magnamedics.com/index.php/magsi-dna. [Accessed: 29-Apr-2018].

[14] Kapelan Media, “SiMAG-DNA,” *SIMAG MPDNA : Magnetic nano and micro particles*, 06-Apr-2007. [Online]. Available: http://www.chemicell.com/products/microparticles/simag-mpdna/index.html. [Accessed: 29-Apr-2018].

[15] Yang D.Y, Waye J.S, Dudar J.C, and Saunders S.R, “Technical note : improved DNA extraction from ancient bone using silica-based spin columns.,” *Am J Phys Anthr.*, vol. 105, no. 4, pp. 539–543, 1998.

[16] C. Katevatis, A. Fan, and C. M. Klapperich, “Low concentration DNA extraction and recovery using a silica solid phase,” *PLoS One*, vol. 12, no. 5, pp. 1–14, 2017.

[17] M. Wierucka and M. Biziuk, “Application of Magnetic Nanoparticles for Magnetic Solid-Phase Extraction in Preparing Biological, Environmental and Food Samples,” *ChemInform*, vol. 46, no. 2, 2014.

[18] Z. M. Saiyed, C. N. Ramchand, and S. D. Telang, “Isolation of genomic DNA using magnetic nanoparticles as a solid-phase support,” *J. Phys. Condens. Matter*, vol. 20, no. 20, 2008.

[19] J. H. Min *et al.*, “Isolation of DNA using magnetic nanoparticles coated with dimercaptosuccinic acid,” *Anal. Biochem.*, vol. 447, no. 1, pp. 114–118, 2014.

[20] Promega, “Calculating Nucleic Acid or Protein Concentration Using the GloMax® Multi+ Microplate Instrument,” *Promega*, pp. 1–6, 2009.

[21] “NanoDrop: How It Works,” *NanoDrop: How it works | Thermo Fisher Scientific*. [Online]. Available: https://www.thermofisher.com/us/en/home/industrial/spectroscopy-elemental-isotope-analysis/molecular-spectroscopy/ultraviolet-visible-visible-spectrophotometry-uv-vis-vis/uv-vis-vis-instruments/nanodrop-microvolume-spectrophotometers/nanodrop-products-guide/nanodrop-how-it-works.html. [Accessed: 30-Apr-2018].

[22] “Quant-iT PicoGreen dsDNA Assay Kit,” *Thermo Fisher Scientific*. [Online]. Available: https://www.thermofisher.com/order/catalog/product/P7589. [Accessed: 08-May-2018].

[23] R. Chand and S. Neethirajan, “Microfluidic platform integrated with graphene-gold nano-composite aptasensor for one-step detection of norovirus,” Biosens. Bioelectron., vol. 98, no. May, pp. 47–53, 2017.

[24] C. Toumazou *et al.*, “Simultaneous DNA amplification and detection using a pH-sensing semiconductor system,” *Nat. Methods*, vol. 10, no. 7, pp. 641–646, 2013.

[25] Y. Cho, J. Lee, J. Park, B. Lee, Y. Lee, and C. Ko, “One-step pathogen specific DNA extraction from whole blood on acentrifugal microfluidic device,” *Lab Chip*, vol. 7, p. 565, 2007.

[26] J. W. Hong, V. Studer, G. Hang, W. F. Anderson, and S. R. Quake, “A nanoliter-scale nucleic acid processor with parallel architecture,” *Nat. Biotechnol.*, vol. 22, no. 4, pp. 435–439, 2004.

[27] I. Iranmanesh, M. Ohlin, H. Ramachandraiah, S. Ye, A. Russom, and M. Wiklund, “Acoustic micro-vortexing of fluids, particles and cells in disposable microfluidic chips,” *Biomed. Microdevices*, vol. 18, no. 4, pp. 1–7, 2016.

[28] M. Rodrigues *et al.*, “Characterization of Passive and Active Microfluidic Devices Manufactured in LTCC Technology,” *Techniques*, pp. 27–29, 2006.

[29] E. A. Schilling, A. E. Kamholz, and P. Yager, “Cell lysis and protein extraction in a microfluidic device with detection by a fluorogenic enzyme assay,” *Anal. Chem.*, vol. 74, no. 8, pp. 1798–1804, 2002.

[30] R. Safavieh and D. Juncker, “Capillarics: pre-programmed, self-powered microfluidic circuits built from capillary elements,” *Lab Chip*, vol. 13, no. 21, p. 4180, 2013.

[31] S. I. De La Cruz-Hernández *et al.*, “Determination of viremia and concentration of circulating nonstructural protein 1 in patients infected with dengue virus in Mexico,” *Am. J. Trop. Med. Hyg.*, vol. 88, no. 3, pp. 446–454, 2013.

[32] “LABORATORIES | HOSPITALS – Virology,” *Biosynex*. [Online]. Available: https://www.biosynex.com/en/laboratories-hospitals-virology/. [Accessed: 25-Apr-2018].

[33] “SD Dengue IgG Capture ELISA,” *SD BIOLINE Dengue IgG capture ELISA - Alere is now Abbott*. [Online]. Available: https://www.alere.com/en/home/product-details/sd-bioline-dengue-IgG-capture-elisa.html. [Accessed: 25-Apr-2018].

[34] “Dengue NS1 Ag Strip #70700,” *Dengue NS1 Ag Strip #70700 | Clinical Diagnostics Bio-Rad*. [Online]. Available: http://www.bio-rad.com/en-uk/sku/70700-dengue-ns1-ag-strip?ID=70700. [Accessed: 25-Apr-2018].

[35] R. A. Martinez-Vega, F. A. Diaz-Quijano, C. Coronel-Ruiz, S. Yebrail Gomez, and L. A. Villar-Centeno, "[Evaluation of PANBIO rapid immunochromatographic cassette for dengue diagnosis in a Colombian endemic area]," *Biomedica*, vol. 29, no. December, pp. 616–624, 2009.

[36] S. D. Blacksell *et al.*, "Evaluation of six commercial point-of-care tests for diagnosis of acute dengue infections: The need for combining NS1 antigen and IgM/IgG antibody detection to achieve acceptable levels of accuracy," *Clin. Vaccine Immunol.*, vol. 18, no. 12, pp. 2095–2101, 2011.

[37] M. O'Neill, J. McPartlin, K. Arthure, S. Riedel, and N. D. McMillan, "Comparison of the TLDA with the nanodrop and the reference qubit system," *J. Phys. Conf. Ser.*, vol. 307, no. 1, 2011.

[38] J. Serth, M. A. Kuczyk, U. Paeslack, R. Lichtinghagen, and U. Jonas, "Quantitation of DNA extracted after micropreparation of cells from frozen and formalin-fixed tissue sections," *Am. J. Pathol.*, vol. 156, no. 4, pp. 1189–1196, 2000.

[39] D. N. Miller, J. E. Bryant, E. L. Madsen, and M. E. T. Al, "Evaluation and Optimization of DNA Extraction and Purification Procedures for Soil and Sediment Samples," vol. 65, no. 11, pp. 4715–4724, 1999.

[40] "Extracting DNA from living things | Nuffield Foundation," *The truth behind SEN statements in mainstream primary schools | Nuffield Foundation*. [Online]. Available: http://www.nuffieldfoundation.org/practical-biology/extracting-dna-living-things. [Accessed: 07-May-2018].

[41] "DNA Extraction from Serum," *Thermo Fisher Scientific*. [Online]. Available: https://www.thermofisher.com/us/en/home/references/protocols/nucleic-acid-purification-and-analysis/dna-extraction-protocols/dna-extraction-from-serum.html. [Accessed: 07-May-2018].

[42] M. Blumenreich, "The white blood cell and differential count," *Clin. Methods Hist. Phys. Lab. Exam. 3rd Ed.*, pp. 724–727, 1990.

[43] O. M. De Bruin and H. C. Birnboim, “A method for assessing efficiency of bacterial cell disruption and DNA release,” *BMC Microbiol.*, vol. 16, no. 1, pp. 1–10, 2016.

[44] B. Freund, M., & Carol, “Factors affecting haemocytometer counts of sperm concentration in human semen. Journal of reproduction and fertility,” *J. Reprod. Fertil.*, vol. 8, no. 2, pp. 149–155, 1964.

[45] P. Desjardins and D. Conklin, “NanoDrop Microvolume Quantitation of Nucleic Acids 2 . High-Sensitivity Microvolume Nucleic Acid Quantitation Using the NanoDrop 3300,” *Jove*, no. November, pp. 1–4, 2010.

[46] A. R. Wheeler and R. N. Zare, “Short communication Electroosmotic flow in a poly(dimethylsiloxane),” pp. 1120–1124, 2004.

[47] H. P. Long, C. C. Lai, and C. K. Chung, “Polyethylene glycol coating for hydrophilicity enhancement of polydimethylsiloxane self-driven microfluidic chip,” *Surf. Coatings Technol.*, vol. 320, pp. 315–319, 2017.

[48] I. Wong and C. M. Ho, “Surface molecular property modifications for poly(dimethylsiloxane) (PDMS) based microfluidic devices,” *Microfluid. Nanofluidics*, vol. 7, no. 3, pp. 291–306, 2009.

[49] N. E. Morton, “Parameters of the human genome.,” *Proc. Natl. Acad. Sci. U. S. A.*, vol. 88, no. 17, pp. 7474–7476, 1991.

[50] “CA46 (ATCC® CRL-1648™),” *CA46 ATCC ® CRL-1648™ Homo sapiens Burkitt's lymphoma*. [Online]. Available: https://www.lgcstandards-atcc.org/Products/All/CRL-1648.aspx?geo_country=gb#generalinformation. [Accessed: 04-May-2018].

[51] “K-562 (ATCC® CCL-243™),” *CA46 ATCC ® CRL-1648™ Homo sapiens Burkitt's lymphoma*. [Online]. Available: https://www.lgcstandards-atcc.org/products/all/CCL-243.aspx?geo_country=gb#generalinformation. [Accessed: 04-May-2018].

[52] "RS4;11 (ATCC® CRL-1873™)," *CA46 ATCC ® CRL-1648™ Homo sapiens Burkitt's lymphoma*. [Online]. Available: https://www.lgcstandards-atcc.org/Products/All/CRL-1873.aspx?geo_country=gb. [Accessed: 04-May-2018].

[53] J. Lachaux *et al.*, "Thermoplastic elastomer with advanced hydrophilization and bonding performances for rapid (30 s) and easy molding of microfluidic devices," *Lab Chip*, vol. 17, no. 15, pp. 2581–2594, 2017.

[54] R. Geuther, "A. L. LEHNINGER, Biochemistry. The Molecular Basis of Cell Structure and Function (2nd Edition). 1104 S., zahlr. Abb., zahlr. Tab. New York 1975. Worth Publ. Inc. $ 17.50," *Z. Allg. Mikrobiol.*, vol. 17, no. 1, pp. 86–87, 2007.

[55] J. M. Bienvenue, N. Duncalf, D. Marchiarullo, J. P. Ferrance, and J. P. Landers, "Microchip-based cell lysis and DNA extraction from sperm cells for application to forensic analysis," *J. Forensic Sci.*, vol. 51, no. 2, pp. 266–273, 2006.

[56] P. Saxena, P. K. Dash, S. R. Santhosh, A. Shrivastava, M. Parida, and P. L. Rao, "Development and evaluation of one step single tube multiplex RT-PCR for rapid detection and typing of dengue viruses.," Virol. J., vol. 5, p. 20, 2008.

[57] Jim Clark, "the Beer-Lambert Law," vol. 39, no. 7, pp. 333–335, 2016.

Appendix 1

A passage number tells you the age of a cell line. At Passage-30, the cells have been “split” or “cultured” in new flasks 30 times.

The figure below demonstrates a 3D image of the chamber volumes.